Development of Compact Mid-Infrared Fibre Laser using 2D-Nanomaterials and Side-Polished Fibre

By

Khadija Karim

A thesis submitted to Macquarie University

for the degree of Master of Research

Department of Physics and Astronomy

October 2019

MACQUARIE University
SYDNEY·AUSTRALIA

Examiner's Copy

This thesis is a presentation of my original research work. Wherever contributions of others are involved, every effort is made to indicate this clearly, with due reference to the literature, and acknowledgement of collaborative research and discussions. The material presented in this thesis is, to the best of my knowledge, original and has not been submitted in whole or part for a degree in any university.

_____

Khadija Karim

Acknowledgements

In the Name of **Allah**, the Most Beneficent, the Most Merciful. All the praises and thanks be to Allah, the Lord of mankind, who gave me the knowledge and strength to work and present my work in the form of this thesis.

I am grateful to my supervisor Alex Fuerbach for the opportunity to carry out this research project. His guidance and mentorship has been a continuous inspiration. He always provided me with useful insights, advice, critical feedback and fruitful discussions during my MRes.

Most importantly, I am grateful to my husband for his love, devotion and patience, which has been truly inspiring. He has always been there for me; without his help I would have not been able to get admission to my university. He is the person to whom I dedicate this thesis.

Starting from the beginning, I thank Gayathri Bharatan, who helped me to shape my research work. I would also like to acknowledge the valuable inputs from my colleague Sobia Rehman. To Peter Dekker, Benjamin Johnston, and Alex Stokes, thank you for your assistance in the lab and, more importantly, for sharing your experience and knowledge.

Now to my amazing colleagues Simon Gross, Joanne Dawson, Martin Ams, Saurabh Bhardwaj and Saheed Oladipupo - it was a great pleasure to work with you all. Furthermore Thanks to Xiantao Jiang and Han Zhang from Shenzhen University, Feng Chen and Ziqi Li from Shandong University to provide support for material printing for the experiment.

Finally, the person I am most grateful to is my mother; because for her continuous love, support and prayers I was able to achieve whatever I have. During my MRes she never asked much from me but gave me all her support. Last but not least, thank you to my sisters, who were always praying and raising my spirits so I could complete this task to the best of my abilities.

This work is a complete mixture of the above people's knowledge and experience.

I thank you all from the core of my heart.

Khadija

Abstract

In the recent past, the field of photonics has opened new horizons and allowed the development of compact photonic devices to replace larger optical devices. This thesis presents a step towards building a compact all fibre mid-infrared laser, using 2D nanomaterials. The experimental setup used erbium-doped double clad ZBLAN fibre as the laser cavity, and an external confocal setup was used to pass the signal through a 2D nanomaterial. The results demonstrated stable mode-locking in the mid-infrared region when we used MXene and $PtSe_2$ 2D nanomaterials as saturable absorbers, while SESAM showed Q-switched mode-locking due to the high band gap energy. The signal to noise ratio of the mode-locked pulses was evaluated against the thickness of the saturable absorber being pasted on the CaF_2 substrate. The results showed an improved SNR, with the increase of the number of layers of saturable absorber resulting in improved mode-locked pulses. Further, the experimental research was extended so as to increase the compactness of the laser through removing the confocal setup and pasting SA on a side polished fibre. For this purpose, we worked to find a reliable and consistent method to side-polish a fibre to access the evanescent field. Custom 3D models were built to precisely side polish a ZBLAN fibre to achieve a smooth surface for nanomaterial printing.

Contents

List of Figures and Tables

List of Acronyms

ETU	Energy Transfer Up-conversion
CW	Continuous Wave
SESAM	Semiconductor Saturable Absorber Mirror
SBR	Saturable Bragg reflector
FET	Field Effect Transistor
TMD	Transition metal Dichalcogenide
FWHM	Full Width Half Maximum
APC	Angle Polished Connectors
ABS	Acrylonitrile Butadiene Styrene
NPE	Nonlinear polarization evolution

1

Introduction

Development in integrated photonics has revolutionized the field of physics and is especially aiming to replace the components of traditional optics. Due to integrated photonics we can confine large optical setups in tiny optical chips, and fibre laser is one of the most important inventions in the field of photonics. Fibre doped with rare earth elements acts as a gain medium in fibre lasers, in which light is coupled due to total internal reflection, and Fibre Bragg grating play the role of reflective mirrors. Lasers in the mid-infrared region are of great significance, especially in the field of molecular spectroscopy, and photonics provides us with an effective solution to create compact mid-infrared fibre lasers for this purpose.

1.1 Motivation

Mid-infrared lasers have proven to be significant in many fields, though especially in molecular spectroscopy for structural identification. The vibrational modes of many common molecular structures reside within the range of the mid-infrared region, so mid-infrared lasers can be used for identification and detection of molecules in various areas, such as hazardous chemical detection, atmospheric monitoring and medicine [1]. With the increase of applications of mid-infrared lasers, research is in progress to reduce the size of these lasers through integrated photonics so as to make them more compact and portable for flexibility of use. In this thesis we will discuss the development of short-pulsed mid-infrared fibre laser through direct integration of a saturable absorber within the fibre laser cavity.

Fibre can be modified to access this evanescent field by removing some portion of the cladding. The interaction of various materials that exhibit saturable absorption (nanomaterials such as MXene and $PtSe_2$) with the evanescent field can be made possible by printing material on to the surface of polished fibre. Side polished fibre (SPF) has been widely used in a variety of applications, including directional couplers, attenuators, polarizers, switches, resonators, filters and evanescent fibre sensors, owing to the well-known evanescent field on the polished fibre surface [2] – [5].

Work is in progress to shrink the laser size which will potentially embed all components of a laser within the fibre. However, a significant challenge in the development of such a laser is to achieve ultra-short pulses for mode-locking. This is only possible through the introduction of 2D nanomaterial, such as MXene and $PtSe_2$, being deposited on the polished side of the fibre. By accessing the evanescent field near the core of the fibre, this field can interact with the saturable absorber. If the material will act as a saturable absorber, losses will be reduced at high power [6] and ultra-short pulses will be generated to achieve the phenomenon of mode-locking, as per the principal of traditional mode-locked lasers. The purpose of the current research is to take a further step towards achieving mode-locking in compact fibre lasers through the interaction of light with materials such as MXene and $PtSe_2$. One of the most important aspect in this regard is to find a reliable method to side-polish a fibre so that the saturable absorber can be deposited onto the fibre so as to achieve the phenomenon of mode-locking within the fibre.

1.2 Thesis Layout

This thesis is divided into five chapters, as outlined below.
This first chapter presents a brief introduction to the thesis topic and discusses the motivation for the work.

Chapter 2 explains the principles of a laser, its components and the concept of a fibre laser. It also explains in detail the phenomena of pulsed lasers, such as Q-switching and mode-locking. It further defines various 2D nanomaterials that are used as saturable absorbers in the experiment.

Chapter 3 explains the development of a pulsed fibre laser using erbium-doped fluoride fibre as a cavity. The experimental setup used 2D nanomaterials (MXene and $PtSe_2$) and a traditional semiconductor saturable absorbers to generate stable mode-locking. The chapter closes with the interpretation of the results achieved from the experiment.

Chapter 4 provides the experimental setup and procedures used to end and side polish a fibre. A custom holder is designed and 3D-printed to secure the fibre for side-polishing. Moreover, a mounting plate compatible with a Logitech PM5 polishing jig is designed to fix the holder. The complete experimental setup is explained in detail that was used to side-polish the fibre using the Logitech PM5, and, finally, the experimental results are discussed.

The thesis concludes with Chapter 5, which discusses potential future work in light of the research work presented in the thesis.

2

Background Theory of Mid-IR Fibre Laser Technology

This chapter explains the principles of a laser, its components and the concept of fibre laser. Rare-Earth ion (such as erbium) doped fibre lasers for the generation of light in the mid-infrared region are of great significance especially because of their diverse applications in spectroscopy. The chapter further explains the importance of saturable absorbers to generate high power ultrashort pulses through the concept of mode-locking.

2.1 LASER

The acronym LASER stands for light amplification by stimulated emission of radiation. The laser was first experimentally demonstrated by Theodore H. Maiman, a scientist at Hughes Research Laboratory in California. The laser was invented based on Einstein's theoretical work and on research by Charles Hard Townes and Arthur Leonard Schawlow. In general, a laser does not only emit visible light but also electromagnetic radiation which is not visible to the human eye, such as infrared or ultraviolet radiation. Initially, the lasers were developed on the basis of emission of microwaves. In early technical literature based on the wave properties, these microwave lasers were called masers, but over time more research introduced lasers based on a diverse range of electromagnetic waves, so the term maser became obsolete. Today, there are a large number of applications of these lasers, especially in optical disk drives, laser printers, DNA sequencing instruments, barcode scanners, fibre-optic and free-space optical communication, skin treatments, laser surgery and cutting/welding materials [7].

2.1.1 Design

The following are the components of a typical laser (refer to Figure 2.1):

1. Gain medium
2. Pump
3. High reflector
4. Output coupler

A typical laser oscillator design is shown in Figure 2.1 below,

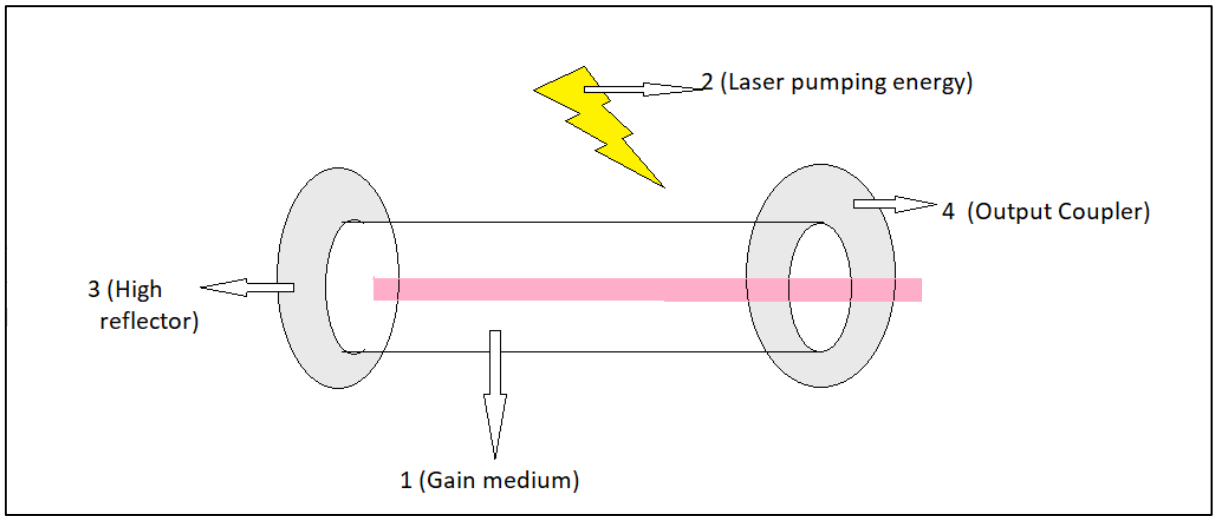

Figure 2.1 Laser oscillator

A laser consists of a gain medium and something to provide optical feedback [2]. The gain medium is the material which provides optical amplification. A light of a specific wavelength passing through this medium gains energy and gets amplified through stimulated emission. The gain medium is supplied with energy (electric or by using light at a different wavelength) through a process called pumping. Pump light can be provided by another laser or a flash lamp. When the light of a specific wavelength passes through this pumped medium, it gains energy and gets amplified.

The most common type of laser uses feedback from an optical cavity, which is a pair of mirrors on both ends of the gain medium; light bounces back and forth between the mirrors and get amplified each time it passes through the gain medium. Typically, one mirror is partially transparent, which is called the output coupler. Some of the light escapes through this mirror, which becomes the output of the laser. In an analogy to electronic oscillators, this device, based on its functionality, is sometimes called a laser oscillator [8].

2.2 Fibre Optics

An optical fibre is a thin thread of glass consisting of a central core surrounded by cladding, where the core has a higher refractive index than that of cladding. The light in the fibre travels at the core-cladding interface by using the phenomena of total internal reflection [9] (Figure 2.2).

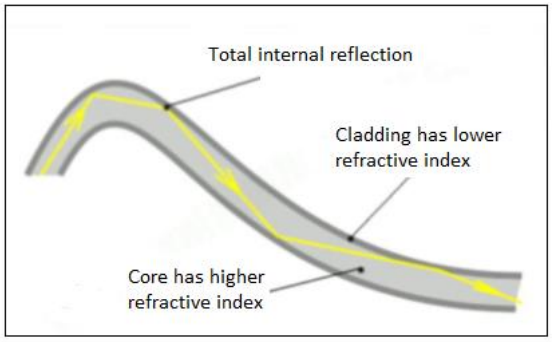

Figure 2.2: Light propagation through fibre

2.2.1 Wave guiding in optical fibre by total internal reflection

As discussed above, optical fibres use the phenomena of total internal reflection. Usually the dielectric fibre consists of a core and a surrounding layer around the core, known as cladding, where the refractive index of the core (n_{co}) is higher than that of the cladding refractive index (n_{cl}), i.e., $n_{co} > n_{cl}$

For a step index fibre, as shown in Figure 2.4, the difference in the core and the cladding refractive indices defines an acceptance cone, which are the set of ray angles that the core will guide via total internal reflection [10].

The sine of the half angle of the acceptance cone is known as the numerical aperture of the fibre, and is written as NA:

$$\text{NA} = \sqrt{n_{co}^2 - n_{cl}^2}$$

To obtain an accurate analysis of the light guiding process, the wave-nature of light has to be considered. We use Maxwell's equation for cylindrical geometry to obtain the discrete solutions of light propagation in the fibre. These discrete solutions within the fibre are known as "modes".

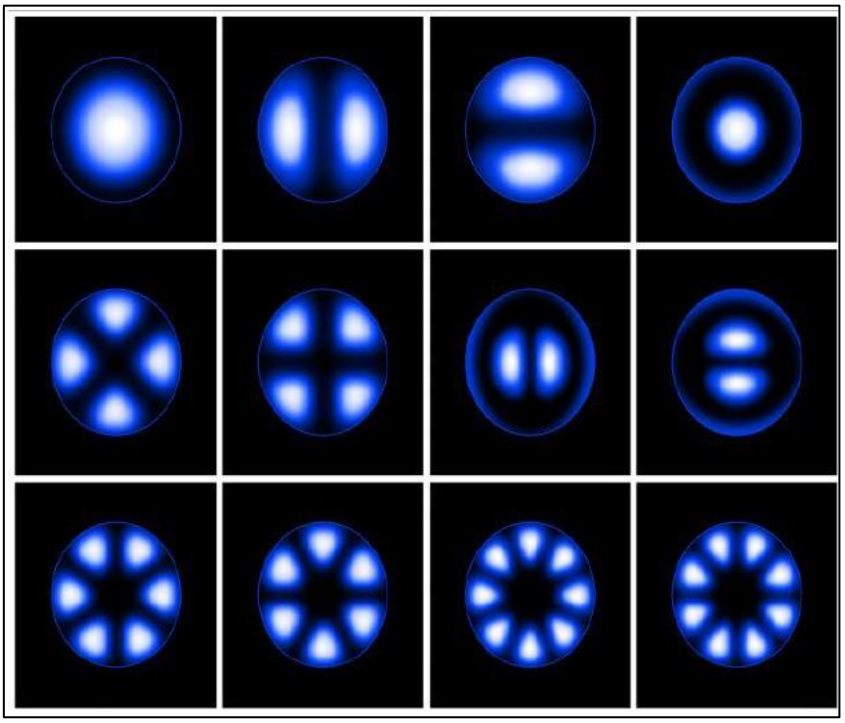

Figure 2.3 Picture shows some of the different modes of fibre

There are discrete numbers of propagating modes existing in a fibre (which is a dielectric waveguide). Another important property of fibre is the "normalized frequency", V, which is related to the number of modes that can be guided in the optical fibre, it should be less than 2.405 for a fibre that only supports propagation of a single mode [8] (i.e., the fundamental mode).

$$\text{V} = 2\pi\text{a}\ (\sqrt{n_{co}^2 - n_{cl}^2})\ /\ \lambda$$

$$\text{V} = 2\pi\text{a NA}/\ \lambda$$

where ‘λ’ is the free space wavelength, ‘a’ is the core radius, and NA is the numerical aperture [11].

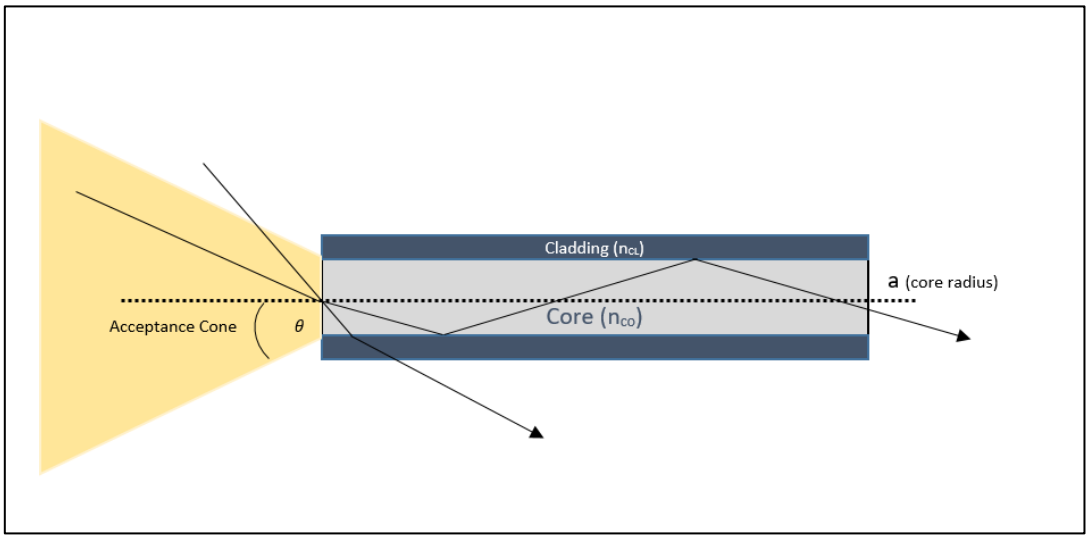

Figure 2.4 Step index optical fibre cross section. The acceptance cone describes the rays the core will guide via total internal reflection, defined by the numerical aperture of the fibre (NA).

2.2.2 Silica versus fluoride fibre

Silica fibre is easier to handle and exhibits rigid properties, such as a high melting point, so it can be used in tough environmental conditions. This is the reason most of the applications including fibre lasers use silica fibre. In the near-infrared region (typically around 1.55 µm), silica fibre shows excellent communication properties due to a low loss (0.2 dB/km) and it allows a broad range of wavelengths to pass through. Due to these properties, Si fibres are used in long distance telecommunication networks. However, these properties tend to deteriorate with an increase in wavelength, and at around 2.5 µm the fibre becomes virtually opaque, so they are not usable at these wavelengths.

As the wavelengths increase (typically after 2 µm) losses start to increase in the silica fibre because the photons absorbed by the silica glass molecules start to generate multiple phonons, and these phonons become the major reason for losses. To avoid this situation, where high phonon energy causes losses, we need to have a propagation material with heavier atoms and a lower bond energy. Fluoride fibres were found to be efficient within the mid-infrared region as they exhibit low phonon energy at longer wavelengths, so they are more suitable for mid-infrared lasers.

Fluoride glass is a multi-composite optical glass composed of several heavy metal fluorides, and many different types of fluoride fibres exist depending on the material composition. Fluoride fibres have many unique characteristics that are not found in silica fibre, such as a wider operating

wavelength range, as well as higher emission efficiency when doped with rare-earth elements. Among many different compositions, two major compositions are ZBLAN fibre (ZrF_4-BaF_2-LaF_3-AlF-NaF) and AlF_3-based fibre (AlF_3-BaF_2-SrF_2-CaF_2-MgF_2-YF_3) [11]. The limitation of fluoride fibre is that it is not easy to handle as it is made up of soft glass with a low melting point. Due to the softness of the material, this fibre is hard to polish and very fragile.

2.2.3 Fibre Lasers

Fibre lasers are the waveguide devices best known for their efficiency and versatility because they use actively doped fibre as a gain medium. A fundamental fibre laser consists of a pump source, an optical feedback element and a gain medium. In a fibre laser, fibre-coupled diodes act as the pump source, fibre Bragg gratings give optical feedback and actively doped fibre core work as gain medium. The main advantage of fibre lasers is their sizes are small, they are low in weight, and they are reliable sources of laser light.

Another important property of fibre laser is their self-cooling capabilities. This is because they have a large surface area as compared to their volume and that is why they can produce high power levels. Furthermore, fibre lasers are highly productive among solid state lasers, and their beam quality is also the optimum. The first fibre laser was developed by E. Snitzer [13] [14] in 1961, and the active medium of this fibre was Nd-doped silicate glass. Because of improved fabrication methods, manufactured fluoride-based and ultralow-loss silica glasses manifest excellent properties, for instance, low scattering, material defects and impurity deficiency. In addition, these properties further improve the quality and quantity of light guided in the fibre.

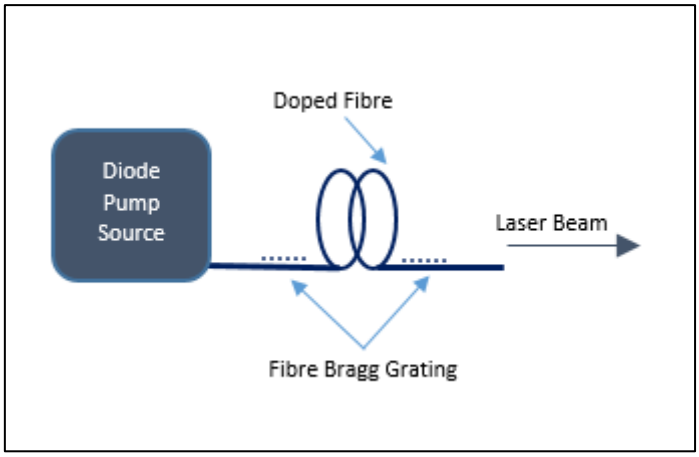

Figure 2.5 Schematic diagram of a fibre laser

2.2.4 Double Clad Fibre

Before starting with the mid-IR fibre laser, the next step is to explore double clad fibres, as they have great importance in the development of a high-power laser system. A low power beam can be easily coupled into the core and the signal can travel through total internal reflection, but as the high-power diodes are used as the pump source, which are of a low beam quality, the coupling of light into the core could be a challenge. Double clad fibre solves this problem through efficient coupling of light. In a double clad fibre, the core has the highest refractive index, followed by the lower refractive index of the middle layer of cladding and the outer layer has the least refractive index.

The light with a low beam quality from a high-power diode gets coupled into the core as well as the middle layer cladding of the double clad fibre. The signal travels into the core through total internal reflection while light also travels into the cladding, and the doped core also absorbs this light from the cladding, thus, improving overall beam quality of the waveguide travelling in the fibre core [15].

2.2.5 Suitable dopant ions for the generation of mid-infrared light

An optical fibre that is capable of transmitting radiation in the infrared region of the electromagnetic spectrum is considered as an infrared optical fibre. The infrared frequency range is from 430 THz to 300 GHz, which is near to microwaves. The infrared wavelengths are further categorized into subclasses of near [0.7 - 2 μm], mid [2 - 20 μm] and far [20 - 1000 μm] infrared. The mid-infrared range is of great importance because of its unique absorption properties, as many molecules exhibit highly specific and strong absorption features in this wavelength range [16]-[20]. Mid-IR optical fibres can broadly be divided into three categories [21]:

- Glasses based on (i) fluorides and (ii) chalcogenides.
- Crystalline materials like (i) sapphire and (ii) halides.
- Hollow fibres having the following categories: (i) glass tube or (ii) hollow core photonic crystal fibres.

All of these classes of fibres are important, but the focus of this project is on glass fibres that are composed of fluoride glass, as this is highly transparent in the mid-IR region of the spectrum.

Many research groups have worked on ZBLAN fluoride fibre lasers doped with different rare-earth ions at different wavelengths. For instance, Allen *et al*. demonstrated that a Thulium ($Tm3^{+}$)-doped ZBLAN fibre laser can emit at 2.3 μm [16], whereas Brinkley *et al*. and Henderson-Sapir *et al*. reported that an erbium (Er^{3+})-doped ZBLAN fibre laser can emit at 2.7 μm and 3.5 μm [17,18]. Moreover, holmium (Ho^{3+})-doped fibre lasers emitting at 2.9 μm, 3.2 μm, and 3.9 μm have been

demonstrated in the past [19-21]. A very recent research paper has demonstrated emissions at 3.26 µm with dysprosium (Dy^{3+}) doping [22]. An overview of the highest output power levels generated by fibre lasers at different wavelengths is presented in Figure 2.6. For the current project, we focus on (Er^{3+})-doped ZBLAN fibre, which is capable of emitting around 2.8 µm as shown in figure 2.6. Fibre lasers, specifically picosecond pulsed lasers, emitting at a wavelength range (mid-IR) from 2.5 µm to 5 µm have gained much attention for their potential applications, such as laser surgery, molecular spectroscopy and micro-machining.

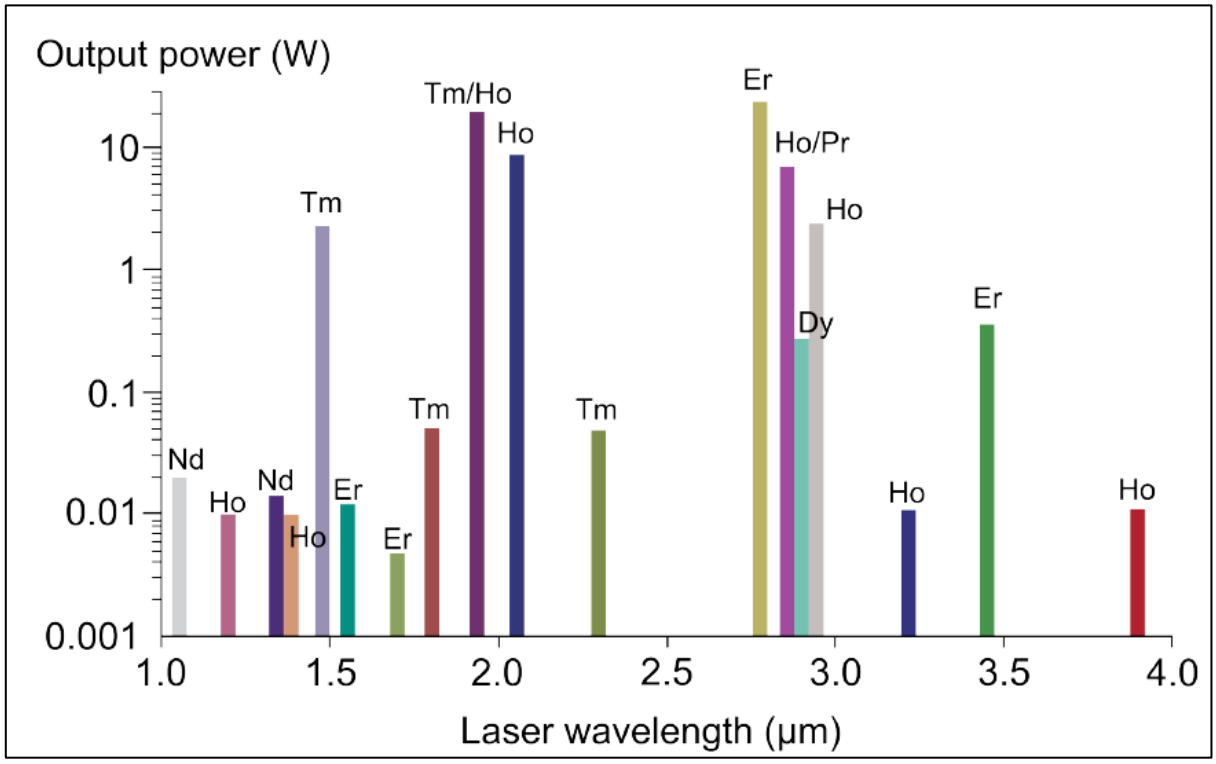

Figure 2.6 various rare-earth ions that have been successfully doped into ZBLAN fibres to achieve lasing

2.2.6 Erbium based fibre lasers

Erbium is one of the rare earth ions which allow efficient generation of 3 µm emission at a high doping concentration. The reason for its efficient emission is the phenomenon of energy transfer up-conversion (ETU). This phenomenon occurs when erbium ions can exchange energy without any external interference due to high doping concentrations, allowing one ion to excite at a higher energy state and the other to stabilize at ground state [23].

Figure 2.7 explains the phenomenon of energy transfer up-conversion. Pumping at 980 nm allows the transition from $^4I_{15/2}$ to $^4I_{11/2}$. $^4I_{11/2}$ state is with a shorter lifespan than $^4I_{13/2}$ and is 6.9 ms, which makes it as self-terminating system causing a 2.75 µm emission and drop to energy level $^4I_{13/2}$. At this level

a high doping concentration of similar ions are capable of exchanging energy between one another without any intervention. So, the energy is transferred to another ion causing one to move at $^4I_{9/2}$ and the other to move at ground state. Ions at ground state continue to interact with pumping light and the process continues. On the other hand, energy state $^4I_{9/2}$ being unstable moves again to $^4I_{11/2}$ through multi-photon release, and from there again a release of 2.75 µm causes the ion to reach the state of $^4I_{13/2,}$ and the process of ETU continues causing a consistent 2.75 µm emission. The process of ions moving to $^4I_{9/2}$ can be referred to as an energy recycling process as the ion again contributes to a 2.75 µm emission [23].

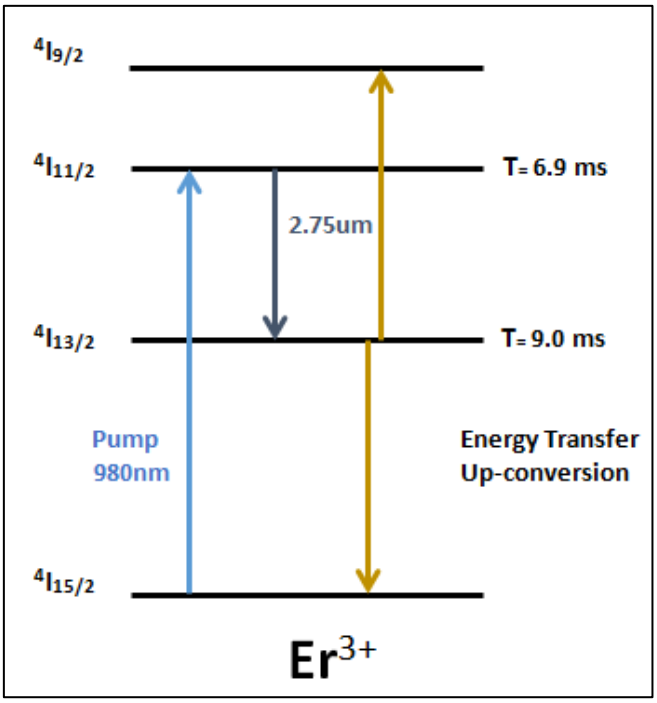

Figure 2.7 Energy level diagram of erbium ions (Er^{3+}). Pumping at 980 nm allows the 2.75 µm transition

2.3 Modes of Operation

Unlike other light, laser light is usually coherent, and it can either be continuous wave or pulsed. Due to these properties, lasers have specialized applications. As the coherence can be different for laser lights, they can be used in various modes of operation to optimize laser performance for various applications.

2.3.1 Continuous Wave Operation (CW)

Laser output in a continuous wave operation remains relatively constant. Helium-neon lasers and carbon dioxide gas lasers are examples of continuous wave lasers where output of the laser is

maintained by a pump source. Some of the semiconductor lasers also generate constant output; thus, they are categorized as continuous wave lasers.

Various factors in a continuous wave laser decide the characteristics of the output light. The gain medium decides the wavelength of light being emitted from the laser. Each output is associated with a line width, which depends on the gain bandwidth of the medium used in the laser and also depends upon the design of the resonator being used to create the phenomenon of inversion population. Neodymium-doped crystals when used as a gain medium lase at a wavelength of 1047 – 1064 nm, while carbon dioxide gas molecules generate 10.6 µm wavelength [24] [25].

2.3.2 Pulsed Operation

The pulsed operation of a laser is where rather than having a continuous power as the output, pulses of certain duration are generated at a certain repetition rate. T.H. Maiman was an American engineer who invented the first laser (pulsed laser) in 1960, which revolutionized the field of optics [26]. In this laser, a chromium-doped sapphire was used as the gain medium, which was pumped by the light of a flashing lamp to generate pulses around the crystal. The wavelength of pulses generated from the setup was 694 nm at room temperature, which was a visible red light. Two sides of the crystal across the axis were coated with silver, which acted as mirrors to trap photons. Light reflected in the cavity back and forth along the mirror axis many times before escaping the crystal.

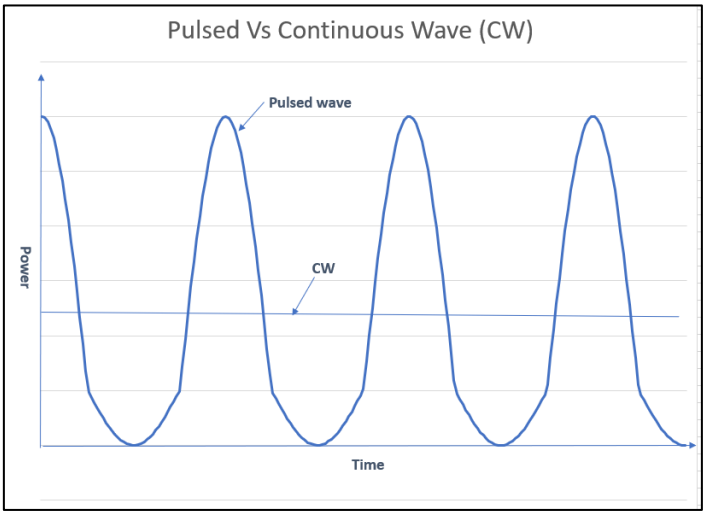

Figure 2.8 Output of a continue waves and pulsed laser.

2.3.2.1 Q-Switching

Q-switching is a process to control the process of stimulated emission within the laser so as to generate high power pulses. Q-switched fibre lasers are probably the most challenging type of lasers in terms of their build and also equally have a high potential for industrial projects. These lasers suffer

from damage due to high power pulse interactions with the surface of the fibre. Control of the laser resonator through Q-switching was first introduced by Hellwarth in 1961[27].

The Q factor is the quality factor, which is used to control the attenuation within the laser cavity, and the idea is to generate short pulses of high power as the attenuation decreases (or the Q factor increases). Initially the attenuation is set to a high loss or low quality factor to disable the laser function, from which the gain starts to build up in the cavity due to population inversion. In the low Q condition, intracavity oscillation is prohibited due to high loss. As the gain in the cavity reaches to its peak, the Q-switch is set from the high loss to the low loss condition (high Q factor), from which power starts to build up in the laser cavity due to the stimulated emission. This causes the population inversion to decrease and after a certain time as the power reaches a certain peak, the laser generates a short duration, high powered pulse through stimulated emission (called a giant pulse or a Q-switched laser pulse) [28].

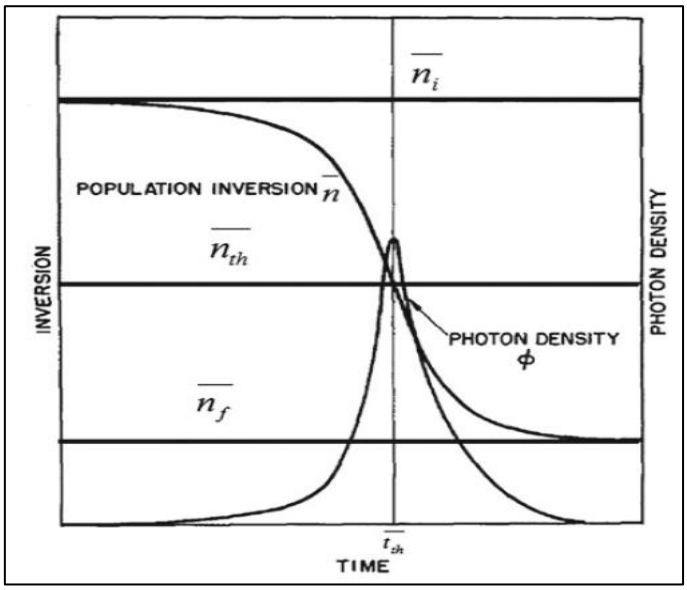

Figure 2.9 Inversion in the Q-switched pulse

Q-switched fibre lasers at 3 μm have already been demonstrated with various active and passive modulation techniques. The first actively Q-switched mid-IR fibre laser near 3 μm was demonstrated in 1994 [56]. An acousto-optic modulator (AOM) and a rotating mirror were used as switching elements in an Er-doped ZBLAN fibre laser. Pulse duration of 100 ns and peak power exceeding 2W were achieved. Tokita, et al. recently reported a 12 W Er^{3+} -doped ZBLAN fibre laser Q-switched by a germanium AOM. Pulses at 2.8 μm with peak power up to 0.9 kW were obtained [57]. Using a TeO_2 AOM, Hu, et al demonstrated a Q-switched Ho^{3+} /Pr^{3+} -codoped ZBLAN fibre laser at 2.9 μm with a pulse width of 78 ns and tunable repetition rate from 40 to 300 kHz [58]. However, an AOM

Q-switched 3 μm laser needs electric equipment for active modulation and careful alignment as well. The gain-switching technique has recently been used in $Er3^{+}$ - and $Ho3^{+}$ -doped ZBLAN fibre lasers to obtain 3 μm pulses [59, 60]. However, gain-switching usually requires high energy pump pulses.

Passive Q-switching based on saturable absorbers which exhibit reduced absorption at high optical intensity is a preferred technique to achieve high intensity laser pulses because it doesn't require additional electric equipment and high pulse energy pumps and has the advantages of simplicity and compactness as well. The first passively Q-switched Er^{3+} doped ZBLAN fibre laser was demonstrated by using InAs epilayers as the saturable absorber [61]. 1.2 μs pulses with energy of 1.25 μJ and peak power of 1.04 W at repetition rate of 1.1 KHz were achieved. Er^{3+} -doped ZBLAN fibre laser passively Q-switched by a Fe^{2+}: ZnSe crystal was reported [62]. 370 ns pulses at 2.78 μm with pulse energy of 2.0 μJ and peak power of 5.34 W were achieved at a repetition rate of 161 kHz. Most recently, $Fe^{2+:}$ZnSe SESAM was successfully fabricated via electron beam evaporation method, where Fe^{2+} was doped into ZnSe layer during the fabricating process. By using Fe^{2+}:ZnSe SESAM in Er^{3+}-doped ZBLAN fibre laser, passively Q-switching laser at 2.78 μm was observed. The stable Q-switched pulses with a pulse duration of 0.43 μs and a pulse energy of 5.43 μJ were generated at a repetition rate of 160.82 kHz, resulting in a peak power of 12.59 W [67].

2.3.2.2 Mode-locking

Mode-locking is a method through which ultrashort pulses are generated in lasers on the order of picoseconds (10^{-12} s) or femtoseconds (10^{-15} s) [29]. The width of these ultrashort pulses range from nanoseconds to femtoseconds, and they are typically produced at a frequency range of 1 MHz to 1 GHz. The qualities or properties of these lasers, such as having high pulse energy, high average power, quality of diffraction limited beam and high repetition rate make these lasers highly important in technological developments. Hargrove et al. gave the first practical demonstration of mode-locked laser in 1964, in which he used an acousto-optic modulator inside a helium-neon laser to achieve mode-locking [30] [31] [32].

A rare earth element doped fibre is used as a cavity for a mode-locked fibre laser. Other components include a pump coupling device, an intracavity modulator, which can be active or passive, and a dispersion compensation device which can be a grating pair. At the start, the setup generates noises, which are short irregular pulses with different phases. These pulses get reflected multiple times through mirrors acting as resonators and get amplified by a laser active medium every time they go back and forth.

There are two ways to generate pulse trains through mode-locked fibre lasers: the laser cavity must contain either an active element or contain a nonlinear passive element. The active element can be an optical modulator, and the nonlinear passive element can be a saturable absorber. Passive mode locking can generate shorter pulses as compared to active mode locking. In active mode locking an acousto-optic or electro-optic modulator or liquid crystal modulator [34] acts as a periodic modulator to generate short pulses. On the other hand, if a saturable absorber is used in a cavity, it reduces losses with the increase in intensity of light because absorption reduces with increased intensity for a saturable absorber, due to which the system can generate as short as femtosecond wide pulses. The losses in the cavity get modulated much quicker in passive mode locking as compared to active mode locking because the saturable absorber is already driven by short pulses, so modulation generates an ultra-short pulse train. The only condition for a saturable absorber is to have a shorter recovery time [33]. The femtosecond laser is one the most important inventions based on passive mode locking, and it is used in very specialized applications such as molecular spectroscopy [34] and advanced micromachining [35] [36].

So from above it can be seen that the pulse train generated in passive mode locking depends upon the material used as the saturable absorber. The first saturable absorber used for mode locking was cryptocyanine in methanol. Since then, many materials have been used to generate shorter and shorter pulse trains. Recently, semiconductors were also used as saturable absorbers, and GaAs was able to generate pulses less than 100 femtoseconds. More and more materials are being researched which can act as efficient saturable absorbers (e.g., carbon nanotubes and graphene).

A material need to go through linear absorption to act as saturable absorber where it initially absorbs energy to become saturated and then do not allow anymore absorption, so acts as transparent for high intensity of light. With the increase in wavelength i.e. moving from near to mid-infrared region we need to have material with lower band gap for linear absorption to make them act as saturable absorbers. This leaves us with fewer choices of material to be used in mid-infrared region as saturable absorbers.

The most commonly used saturable absorber in the mid-IR region is the semiconductor saturable absorber mirrors (SESAMs) [63-65]. Though SESAMs are currently the most prevalent saturable absorbers and have shown their capability for mode-locking mid-IR fibre lasers in the 3 μm region, they usually have a narrow operating wavelength range and require complex fabrication and packaging. Another kind of saturable absorber in the mid-IR region is the transitional metal doped crystals such as Fe^{2+}: ZnSe and Fe^{2+}: ZnS crystals. These saturable absorber crystals possess the

advantages of large absorption cross-section, small saturation energy (low saturable loss) and excellent opto-mechanical properties (damage threshold ~2 J/cm^2). However, these crystals have long relaxation time and may not be suitable for passive mode-locking.

A 3 μm self-Q-switched wavelength-tunable Ho^{3+}: ZBLAN fibre laser has already been demonstrated by using a 2 m Ho^{3+}: ZBLAN fibre as gain media and a pair of fibre end-facet mirrors (M1 and M2) to assemble the laser cavity. The 3 μm fibre laser can delivered stable self-Q-switched pulses while maintaining a compact all-fibre configuration. Output power in given mentioned setup is still limited but have potential to create tunable 3 μm Q-switched pulses from a compact all-fibre laser system [68].

Extensive research is in progress for development of compact mid-IR all fibre laser and following are the successful achievement so far.

- In 2014, a passively mode-locked $Ho^{3+}Pr^{3+}$ -doped fluoride fibre laser was demonstrated to produce 6 ps pulses at a repetition rate of 24.8 MHz, with a peak power of 465 W. A ring cavity was demonstrated in a fluoride fibre laser arrangement which was essential to the generation of stable and self-starting mode-locked pulses [70].
- In 2015, stable soliton pulses were demonstrated from a passively mode-locked ring laser that included a 3 m piece of Er^{3+}: fluoride fibre. The simple mode locking system based on nonlinear polarization evolution (NPE) in the fibre enabled the production of 207 fs pulses with 3.5 kW of peak power emitting around 3 μm. The demonstration was a major step toward the development of efficient femtosecond fibre sources operating in the mid-IR region [71].
- In 2018 a new approach to mid-IR picosecond pulse generation from a compact fibre system was demonstrated. Spectral coverage of 2.97 to 3.30 μm with stable pulses of 33 ps and up to 2.7 nJ energy were achieved. This performance was achieved by leveraging the remarkable spectroscopy of dysprosium-doped fluoride fibres and the understudied frequency shifted feedback pulse generation mechanism. The long wavelength and broad spectral coverage of such mode-locked laser opened further opportunities in the mid-IR [72].

The following discusses two different 2D nanomaterial and semiconductor saturable absorbers used for our experiment.

- **SESAM (Semiconductor Saturable Absorber Mirror):**

  Various types of Lasers use SESAM for generation of ultra-short pulses through demonstration of passive mode-locking. A semiconductor saturable absorber mirror is a

structure with incorporated saturable absorber. A SESAM is composed of a Bragg mirror with a single quantum well absorber layer near the surface.

No absorption occurs near the Bragg mirrors as they have high band gap energy so most of the light reflects from this region. This is the reason that SESAM is also sometimes called saturable Bragg reflectors (SBRs). The device life time can be improved using a suitable passivation layer on top surface of the layer. A large modulation depth for passive Q-switching can also be achieved by using a thicker layer of absorber [37].

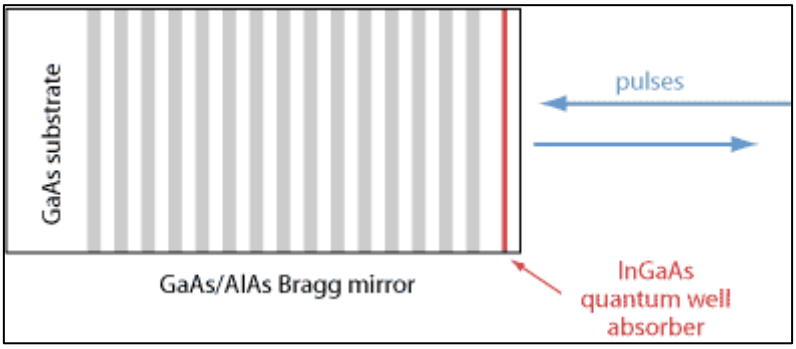

Figure 2.10 Structure of a typical SESAM for operation around 1,064 nm. On a GaAs substrate, a GaAs/AlGaAs Bragg mirror is grown. Within the top layers, there is an InGaAs quantum well absorber layer, which may be, e.g., 10 nm thick

- **$PtSe_2$**

Platinum diselenide, when used as a multilayer film, has been experimentally tested as a saturable absorber. $PtSe_2$ has a high band gap but when used as a layered film its band gap tends to decrease, and a bulk layered film of material has a zero-band gap [37]. A multilayer platinum diselenide ($PtSe_2$) film was experimentally demonstrated as a new type of saturable absorber. The carrier mobility of $PtSe_2$ is the highest among transition metal dichalcogenide **(**TMD) materials. Moreover, the stability of this material in air is excellent. Due to these properties, this material has been used in diverse applications such as FETs (Field Effect Transistors), photodetectors and photo catalysis [39].

- **MXene:**

Nanomaterials are another dimension of research to explore in relation to the development of saturable absorbers. Recently, nanomaterials such as graphene and carbon nanotubes have gained a lot of attention from researchers for the development of SAs. 2D nanomaterials, such as graphene, have shown exceptional properties as saturable absorbers. MXene is another new

2D material which is of great importance because of its electrical and optical properties [38]. MXene is a combination of elements, which can be represented with the following generalized formula:

$M_{n+1}X_nT_x$

M can be any transition metal such as Ti.

X is Carbon and/or Nitrogen

T is Surface Terminations, such as Oxygen and Fluorine

n = 1, 2, or 3

MXene has been mostly researched experimentally or theoretically for its linear properties as well as nonlinear properties. As it is a 2D crystal material, MXene has gained importance for its applications in ultrafast photonics, electromagnetic interference shielding and energy storage [38]. We have used Ti_3C_2Tx which is one of the type of MXene that has been used throughout this research and we would like to thanks a group of Shenzhen University, China for providing us with the required sample of MXene for this purpose.

In recent research all-fibre erbium-doped soliton and dispersion-managed lasers, with a soliton-pulse of 597 fs and stretched-pulse of 104 fs, mode-locked using a microfibre-based MXene SA device has been fabricated via an optical deposition method, which has demonstrated the shortest pulse duration achieved using MXene in a fibre laser (104 fs). Following table shows the results achieved [69].

Material	Output Power (mW)	Central Wavelength (nm)	Spectral Width (nm)	Pulse Duration (fs)
Ti3C2Tx	3	1555.01	22.2	159
Ti3C2Tx	0.285	1564.24	5.21	597.8
Ti3C2Tx	1.3	1550	42.54	104

Table 2.1 Output Performance Comparison of the Er-Doped Fibre Lasers Based on MXene ($Ti_3C_2T_x$) SA Materials [69]

Work is in progress to test various 2D materials on side polished fibre to achieve stable mode-locking for the purpose of development of compact mid IR fibre laser. Table 2.1 shows results achieved by depositing various 2D materials on side-polished fibre for mode-locking.

2D Material	Incorporation Method	Central Wavelength (nm)	Pulse Duration (ps)	Repetition Rate (MHz)	Pulse Energy (nJ)
Bi_2Te_3	Deposited on side-polished fibre	1935	0.795	27.9	0.72
Bi_2Te_3	Deposited on side-polished fibre	1909.5	1.26	21.5	--
MoS_2	Saturable absorber mirror	1905	843	9.67	15.5
WS_2	Deposited on side-polished fibre	1941	1.3	34.8	0.0172
WTe_2	Deposited on tapered fibre	1915.5	1.25	18.72	2.13
BP	Deposited on fibre end	1910	0.739	36.8	0.0407
Bi_2Te_3	Saturable absorber mirror	2830	6	10.4	8.6
BP	Saturable absorber mirror	2783	42	24	25.5

Table 2.2 Performance Summary of Mode-locked Mid-IR Fibre Lasers Based on various 2D Materials [66]

Inkjet printing is a forefront technique to exploit the merits of 2D materials for printed optoelectronic devices with small-footprint, integration, substrates/geometrics compatibility, scalability, and low cost. The choosing of ink solutions is regarded as the key point. High viscosity solution like N-methyl-2-pyrrolidone (NMP) and dimethyl sulfoxide (DMSO) are normally used in the 2D material liquid exfoliation processes, and thus can be directly used for ink formulation. However, high temperature annealing after-treatment may be incurred to remove the polymers which will impair the performance of 2D crystals. Single or mixed low boiling point alcohols (e.g. ethanol, 2-butanol, isopropanol) and biological compatible water are also proposed as the ink solutions with careful ink surface tension and viscosity engineering . A small amount of polymers or proteins can also be added into the solutions that act as “binders” to improve the printed film uniformity.

In chapter 3 we used metallic titanium carbide $Ti_3C_2T_x$ MXene and prepared via acid etching approach. Low boiling point, non-toxic, “binder-free” MXene nanosheets ink is formulated using isopropanol (IPA, boiling point 82.6°C) for establishing functional devices on silica glass, SiO_2/Si wafer, side-polished fibre, flexible and transparent PET film, and gold mirror substrates.

3

Experimental Setup for Stable Mode-locked Mid-Infrared Fibre Laser

This chapter explains the experimental procedure used to generate stable mode-locked pulses in a mid-infrared fibre laser using 2D saturable absorbers, such as MXene and $PtSe_2$. Chirped fibre Bragg grating was used to provide a wavelength stability to demonstrate the mode-locked fibre laser [40]. Multiple components external to the fibre were used to pass the signal through the 2D nanomaterial. These components were built using CaF_2, which acts as a transparent material for the mid-infrared region and, thus, poses no losses to the signal passing through it, but, however, is a hurdle towards the compactness of the fibre laser. The next chapter (Chapter 4) will discuss an improvement for this limitation.

3.1 Mid-Infrared Fibre Laser Experimental Setup

Figure 3.1 explains the experimental setup used to demonstrate stable mode-locking through the use of a Fabry-Perot laser cavity. A four-meter double clad ZBLAN fibre (8 micron core and 125 micron cladding) doped with Erbium ions with doping level 60,000 ppm was used as the laser cavity. The fibre was connectorized at the input end, to minimise the coupling losses, to a commercially available 980 nm pumping source. Fibre was coupled whereas fibre diameter was 100micron and the maximum power level was 5w. Chirped fibre Bragg grating was written at the input of the fibre using the femtosecond laser direct write method [40] [41]. Reflectivity of this fibre Bragg grating was 93%, with a bandwidth of 3 nm to provide wavelength stability. The output of the fibre was angle cleaved to avoid Fresnel reflection (to avoid lasing off the facet) so that light could be transmitted to an extended portion of the cavity so as to interact with the 2D nanomaterial.

A pump filter was used at the output of the fibre to separate the signal from the unabsorbed pump wavelength. After the pump filter, an optical setup of CaF_2 lenses with a focal length of 12.5 mm was used and a 2D saturable absorber was placed between the two lenses. The first lens was at a distance of 2F from the 2D nanomaterial, where F is the focal length (i.e., at 12.5 x 2 mm). This lens focuses the wave right on to 2D nanomaterial, and after the light passes through it, the next lens is placed at F (i.e., 12.5 mm), which collimates the light onto an optical coupler. The optical coupler is used to couple the light from the lens into a detection system through a mirror.

Two samples of mid-infrared saturable absorbers were created using CaF_2. The significance of CaF_2 is that it works as a transparent material for the mid-infrared region and, thus, allows all the light to pass through without any intrusion. One of the samples was generated through ink-jet printing of MXene ($Ti_3C_2T_x$) on a CaF_2 substrate, and the second was synthesized by chemical vapour deposition (called CVD) of $PtSe_2$ on CaF_2. Chemical vapour deposition is a method where material gets decomposed and deposited on the surface of the substrate through a chemical reaction. This process is usually thermal driven. PtSe2 was deposited using CVD, as it responds better to the chemical deposition. Inkjet printing is a relatively modern method for depositing large layers of materials on the substrate through the preparation of the ink with the material to be pasted so as to achieve more consistent surface patterns. The experiment was also conducted by using SESAM, a commercially available semiconductor saturable absorber used in various industrial applications.

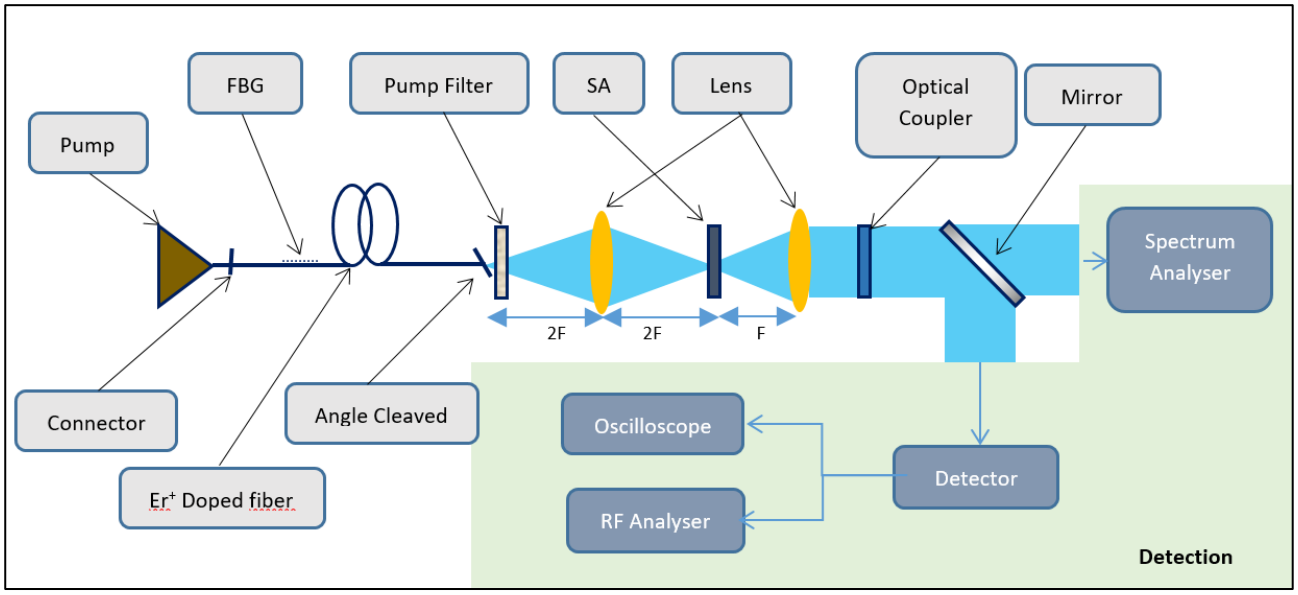

Figure 3.1 Experimental setup to achieve mode-locked pulses in fibre lasers.

The last component of the Fabry-Perot laser cavity was a 50% output coupler, which provided the output of the cavity to be delivered to various detection systems. These detection systems were used to analyse the spectrum of the output beam, power levels and the RF spectrum of the output beam of the laser cavity. The output for both $PtSe_2$ and MXene was recorded, and stability was found to improve with the increased layers of $PtSe_2$ and MXene on CaF_2. $PtSe_2$ was deposited with 4, 6, 8 and 10 layers on CaF_2, while the MXene layers printed on CaF_2 were 3, 4, 6, 8, 12 and 16. This was a collaborative work, and samples were prepared in China by a group of students through chemical vapour deposition and inkjet printing for $PtSe_2$ and MXene, respectively.

3.2 Results and Discussions

Results were recorded for multiple samples used as saturable absorbers. A commercially available saturable absorber SESAM was also used in the experimental setup to verify its properties to generate mode-locking.

3.2.1 Output optical spectrum

The setup shown in Figure 3.1 was used to repeat the experiment with various samples of saturable absorbers. One of the most important aspects to observe was the difference in the spectrum due to the introduction of a saturable absorber. For this purpose, the experiment was first conducted without any material between the confocal setup, and the results were recorded. The results suggested an increase in bandwidth due to the introduction of a saturable absorber.

Figure 3.2 shows the comparison results where the wave is centred at 2,796 nm. The bandwidth for both the signals was measured through the method of Full Width Half Maximum (FWHM), where it is measured at half of the peak power of the signal. Most of the frequencies constituting the signal are captured within this band defined by FWHM. The spectrum width measured with the saturable absorber was found to be 721 pm, while without the saturable absorber, the signal had a narrower band of 464 pm, suggesting a spectral broadening of 257 pm, which is a 55% increase as compared to the signal without the saturable absorber. This increase in the spectrum suggested a decrease in pulse duration in time, and this is due to the introduction of a saturable absorber within the setup. In Section 3.2.3.2, we will use these results to calculate the pulse width of the signal.

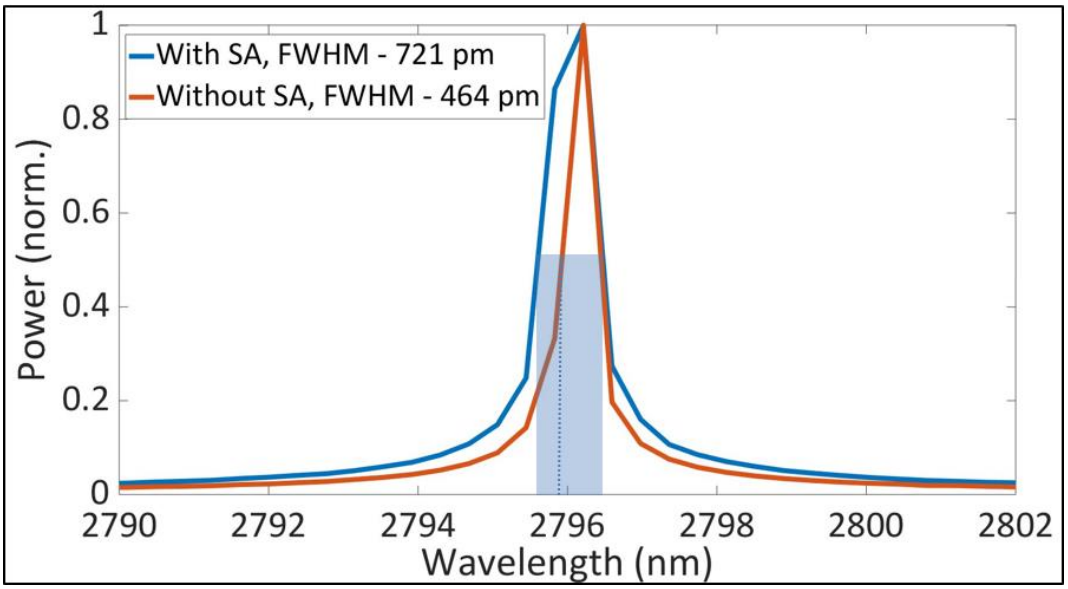

Figure 3.2: Bandwidth spectrum of output with and without SA (with 100 Pico meter resolution of FTIR)

3.2.2 Result of SESAM

In the setup shown in Figure-3.1, we used a commercially available SESAM (BATOP GmbH, Germany) to evaluate the setup's effectiveness for mode-locking. The results from the SESAM were found to favour Q-switched mode-locking rather than CW mode-locking. A typical Q-switched mode-locked pulse has shorter pulses of around a megahertz repetition rate, while the Q-switched envelop is within a kilohertz repetition.

Even though SESAM is a commercial used saturable absorber, and it is an effective tool for generating stable mode locking in near-IR, results suggested that SESAM becomes less efficient in the mid-infrared region [42]. The results are shown in Figure 3.3 for the mid-IR region.

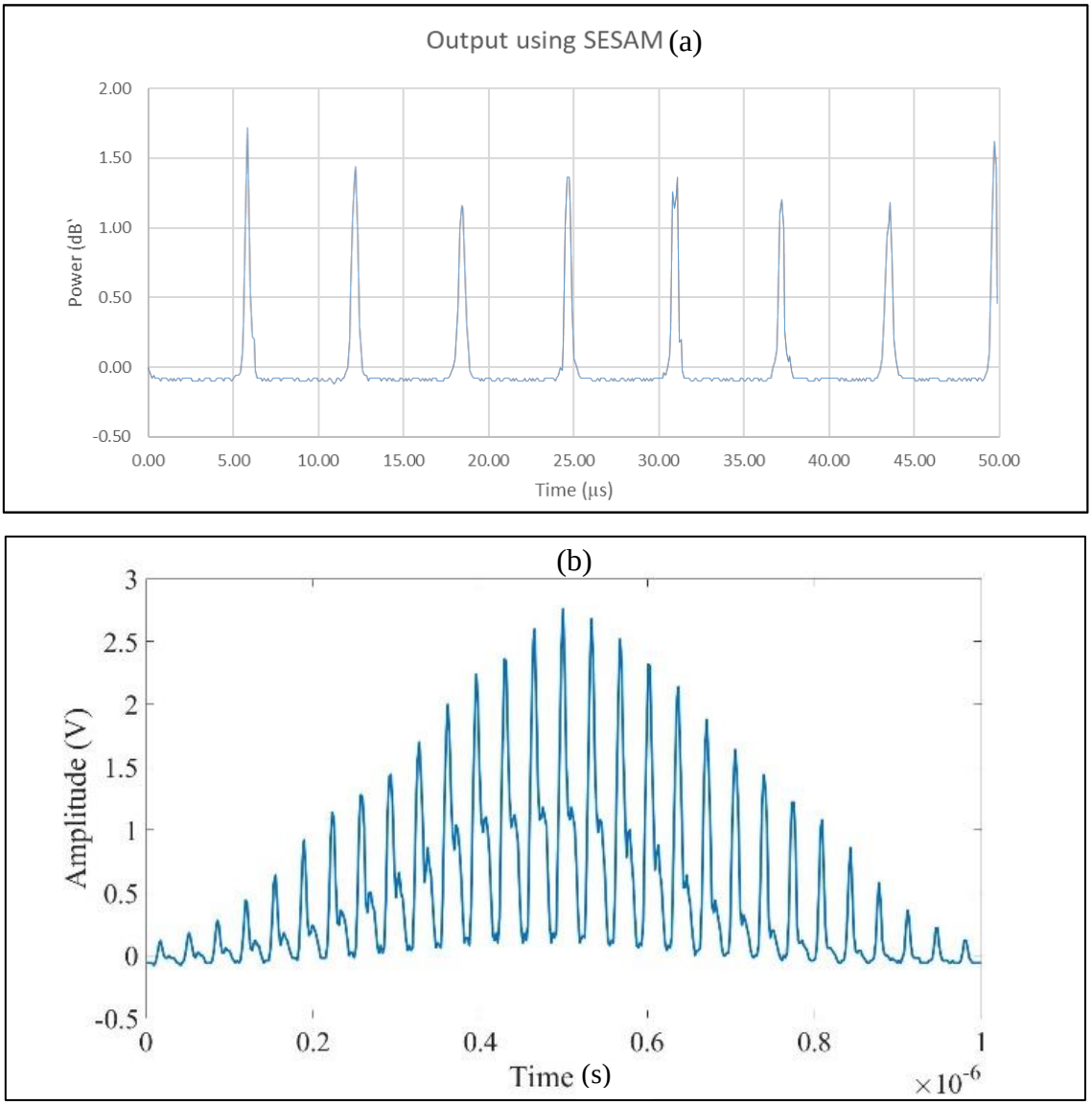

Figure 3.3 Pulse train achieved by using SESAM as saturable absorber: (a) pulse output (b) a zoom in version of envelop of 1µs (oscilloscope view).

The graphs above suggest that pulse energy is not constant, and ultra-short pulses are generated under a Q-switched envelop. The Q-switched envelop shows a repetition rate of around 150 KHz, while the short pulses within each of this Q-switched envelop show a repetition rate of 30 MHz. These results demonstrate the phenomenon of Q-switched mode-locking (QML), where the pulse train, rather than having a constant power, follows a modulated signal pattern with a strong peaked Q-switched pulse. These Q-switched instabilities are unwanted in many applications where a constant pulse power is required. Section 3.2.3, below, will explain the demonstration of stable mode-locking using 2D nanomaterial.

3.2.3 Results of $PtSe_2$ and MXene

We tried novel 2D nanomaterials, such as $PtSe_2$ and MXene, in our laser cavity. $PtSe_2$ was deposited on the CaF_2 substrate at 1 mm thickness. As detailed earlier, this was a collaboration work, and one of the Chinese groups helped to deposit the 2D nanomaterial ($PtSe_2$) on CaF_2. We deposited various layers of $PtSe_2$ on multiple CaF_2 samples in order to see how it performed in our laser cavity (shown in Table 3.1). Stability increased with the increase in the number of layers of nanomaterial on CaF_2. Multiple samples were created through the inkjet printing of various layers of MXene on CaF_2 substrate (see Table 3.1 above). Figure 3.4 shows the output signal as the number of layers of MXene change.

The output was a stable train of pulses with power of 340 mW at a repetition rate of 30 MHz for 16 layers of MXene, as shown in Figure 3.4 below. The output power when we used three layers of MXene was around 250mW, which was at the same repetition rate as it was for 16 layers.

The other reason for high SNR in higher layers is low power distribution across noise. It can be clearly seen from Figure 3.4 (a) that there were multiple strong repetitions of unwanted pulses as well, while in Figure 3.4 (b) the power is mostly distributed within our signal of interest, causing the overall peak power to increase and reducing the power of unwanted signals; thus, demonstrating stronger mode-locking phenomenon. Results were found to be almost similar for $PtSe_2$, and increments in layers improved the mode-locked pulses.

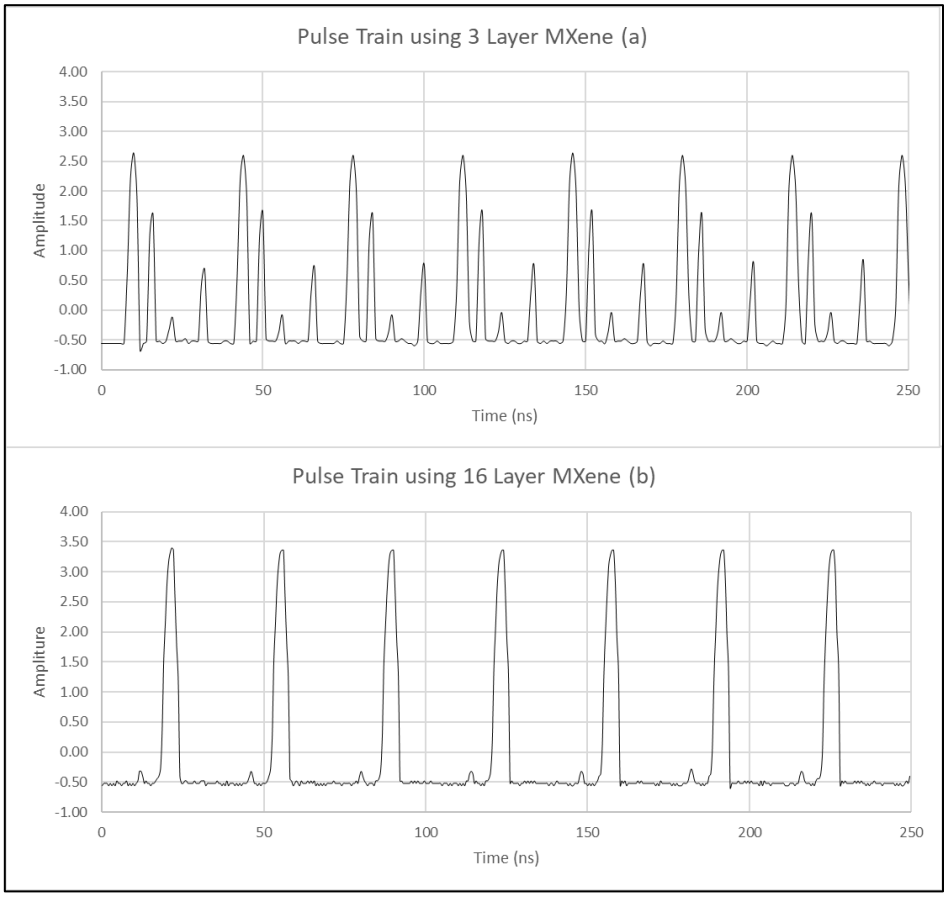

Figure 3.4 Output comparison of 3-layer and 16-layer MXene: (a) 3-layer sample output (b) 16-layer sample output.

3.2.3.1 RF-Spectrum analysis

For the purpose of better understanding the pulses generated through mode-locking we needed to analyse the Fourier Transform of the signal. A limited bandwidth or a limited transform pulse is a pulse with a minimum possible duration within a bandwidth, which can only be achieved through high power, ultra-short pulses generated in mode-locking [43]. Bandwidth limited pulses usually have harmonics in phase, which converge to generate high power ultrashort pulses. Figure 3.5 shows the signal in the frequency domain for a 4-layer and a 12-layer sample used in the fibre cavity. The first observation from both the graphs to be made is the attenuation in amplitude as we moved to the higher frequency, which is caused by the detector roll-off. Also, the signal is only available until 2.2 GHz in both graphs, which is a limitation of our detector.

The signal for both samples shows a peak repetition rate of 30 MHz (as demonstrated in time as well). In a 4-layer sample, we experienced a signal to noise ratio of almost 40 dB, which is due to the high power of other frequencies (considered noises) present in the signal. On the other hand, the signal to noise ratio of the 12-layer MXene was almost 70dB, which means irrelevant frequencies used lower power and, thus, resulted in a stronger signal. Due to detector roll-off we cannot even detect the signal

in Figure 3.5 (a) after 1.5 GHz, while in Figure 3.5 (e) the signal can be easily detected even after the rolling-off effect till 2.2 GHz.

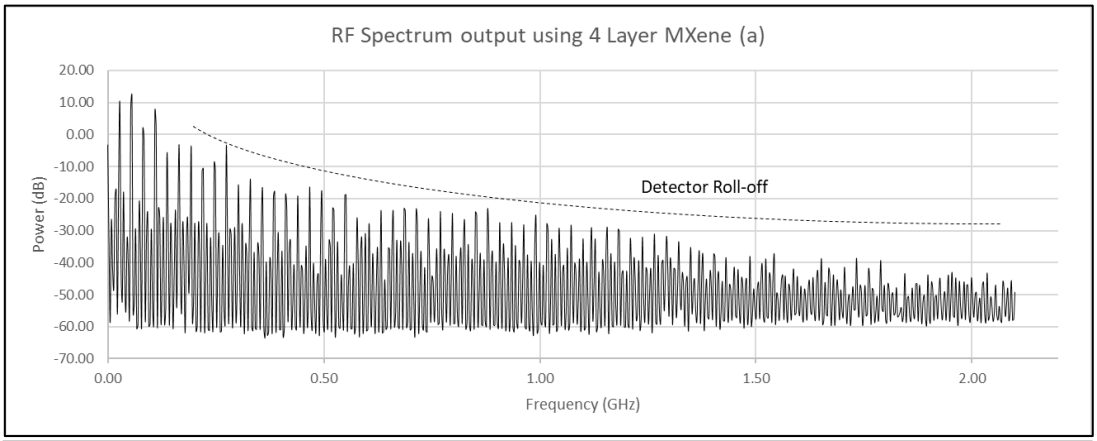

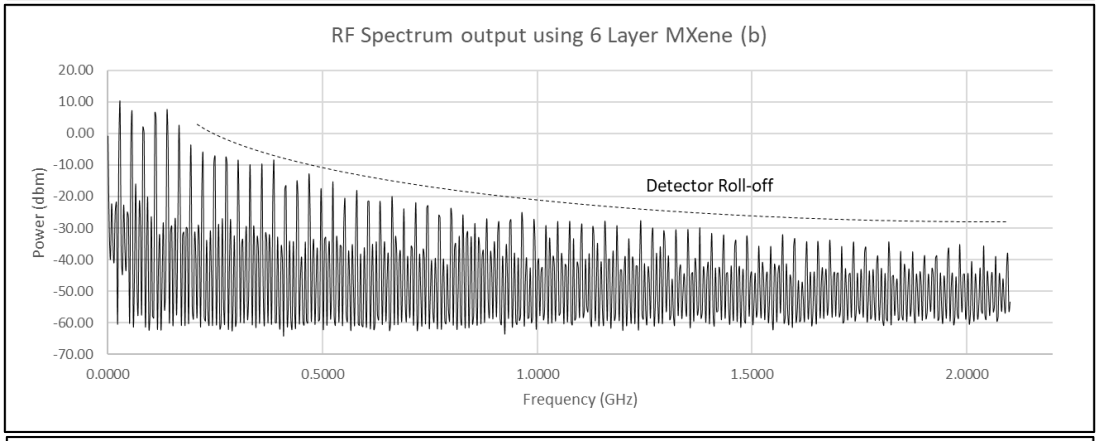

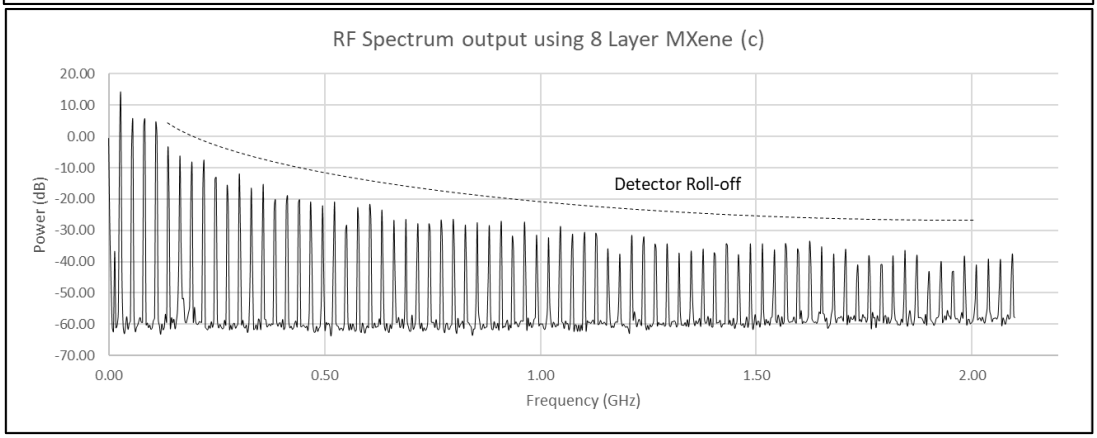

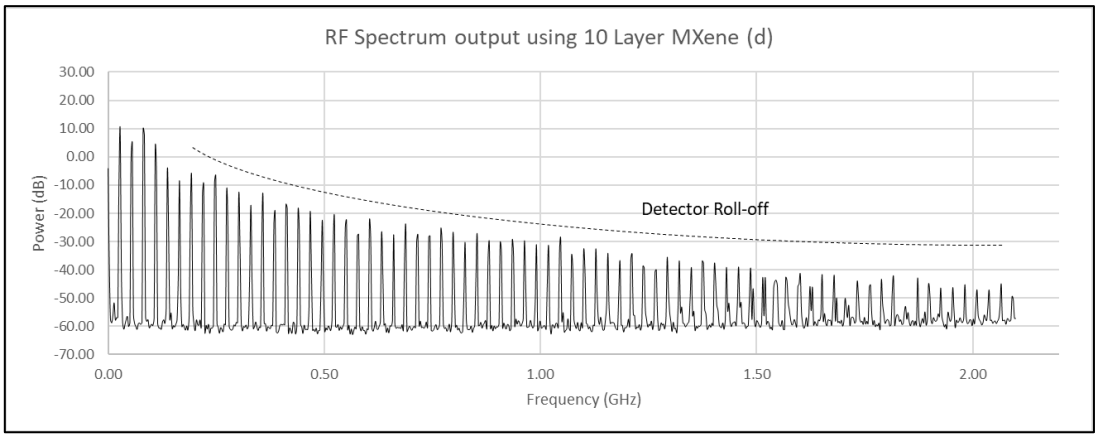

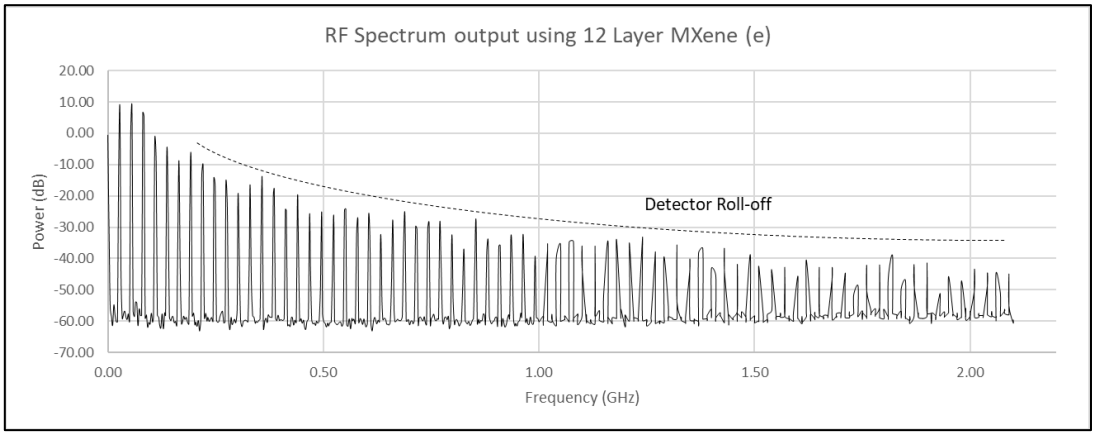

Figure 3.5 RF spectrum of MXene demonstrating mode-locking: (a) 4-layer MXene sample (b) 6-layer MXene sample (c) 8-layer MXene sample (d) 10-layer MXene sample (e) 12-layer MXene sample

The graphs in above figure show performance of 5 samples being used in experiment with varying layers of MXene. It can be clearly seen from RF spectrum that signal to noise ratio increases with the increase in number of MXene layers being used in the setup. In Figure 3.5 (a) and (b) with 4 and 6 layers of MXene respectively, we can hardly segregate signal from noise especially at higher frequency with detector roll-off factor increasing. Figure 3.5 (c), (d) and (e) signal improves with increasing number of layers of MXene which implies that higher number of layers of MXene act as a better saturable absorber t achieve desired results in mode-locked laser.

3.2.3.2 Pulse width measurement

With the help of all wave data available we could estimate the pulse width. TBP (time bandwidth product) was used to estimate the minimum pulse width. As we can see from Figure 3.2, the output spectrum is a normal distribution, so the wave pattern is of a Gaussian wave. For Gaussian waves the TBP can be given by the following equation [43]:

$$\Delta\nu.\Delta\tau \approx 0.44$$

The significance of this relationship is that in bandwidth limited signals (which we assume to have in this scenario), bandwidth is inversely proportional to the width of the pulse. This means that the lesser the width of the pulse, the greater is the bandwidth of the signal (and, thus, more harmonics with the same phase strengthen the pulse frequency). As we already have the normal distributed wavelength graph of the signal, we can use the parameters in the wavelength. The frequency and wavelength relationship can be given by the following equation:

$$\Delta\nu = \frac{c}{\lambda^2}\Delta\lambda$$

Here $\Delta\lambda$ is the FWHM of the wavelength spectrum, which is 721pm for the signal with the saturable absorber, while λ is the base wavelength with peak power, which is 2.796 µm as per the graph in Figure 3.2, so we can calculate $\Delta\nu$ from these values:

$$\Delta\nu.\Delta\tau \approx 0.44$$

$$\Delta\tau \approx \frac{0.44}{c} \times \frac{\lambda^2}{\Delta\lambda}$$

$$\Delta\tau \approx 15.90 \text{ ps}$$

3.3 Chapter Summary

To conclude, we were able to achieve stable mode-locking in mid-infrared fibre lasers using novel 2D saturable absorbers. A pulse train of 30 MHz with 350 mW of power was captured at the output of the laser. This is an important step towards the development of an all fibre laser setup. The large optical cavity has been replaced by a doped ZBLAN fibre with grating acting as the mirror. Moreover, the issue of light coupling was also resolved by using double clad fibre, and with this setup, diodes with low beam quality can also be used as the pump source. Some optical elements, such as a mirror, lenses and optical couplers still pose a constraint to achieving a compact size of the laser and high-quality output pulse train.

A high-power passively Q-switched Er^{3+} doped ZBLAN fiber laser is already demonstrated using SESAM as a saturable absorber. Stable Q-switched fiber laser pulses with a pulse duration of 0.45 µs, a pulse energy of up to 10.82 µJ, a peak power of 24.45 W and a maximum average output power of 3.01 W at a repetition rate of 278.5 kHz was obtained through the passively Q-switched directly which was the highest currently reported average output power from direct passively Q-switched fiber lasers based on a SESAM in the 3 µm wavelength region [73]. But so far no significant research has been conducted towards usage of saturable absorber to achieve stable mode-locking in mid-infrared all fiber laser. The experiment demonstrated above opened new dimensions to achieve mode-locking in all fiber laser using 2D nanomaterial in mid-infrared region.

Chapter 4 will detail the reliable method used to side polish the ZBLAN fibre so that 2D nanomaterial saturable absorbers can be pasted directly on the polished surface of the fibre, and, thus, to interact

with the waveguide through the evanescent field of the fibre to achieve the mode-locking phenomenon.

4

Experimental Setup to Side-Polish Fibre for Mid-Infrared Fibre Lasers

Chapter 4 elaborates on Chapter 3 and provides an extension to improve the experimental setup used in Chapter 3. Rather than having lenses and a 2D saturable absorber layer as external independent components, we side polished a fibre to deposit a saturable absorber, which we expect to have behaviour similar to the experimental setup used in Chapter 3. To gain access to the field around a fibre core (evanescent field) we need to remove some portion of the fibre cladding. Before side-polishing we need to create an experimental setup, where we have to connectorize the fibre from both ends so that a source (Mooseine 1550nm Single Mode Laser Light Source) and meter (power meter - 0.01dB resolution, calibrated at 1550 nm) can be attached to the fibre for monitoring purposes. So, this chapter is split into two sections: The first section discusses the facet polishing of a fibre and the second section describes the side polishing of a fibre. Side polishing and grinding of a fibre is of great significance for the development of mid-infrared lasers.

4.1 Experimental Procedure

4.1.1 Sample pre-processing

As already explained in Chapter 2 optical fibre consists of three basic elements: core, cladding and outer coating, and the light transmission portion of the fibre is a core which has a higher refractive index in comparison to cladding. The cladding is usually made of a similar material to that used in the core but has a slightly lower refractive index; because of this index difference light is confined within the core through the phenomenon of total internal reflection [44]. The preparation of the sample usually starts with stripping both ends of the fibre, followed by connectorization and facet polishing.

4.1.2 Fibre stripping

The polymer of Si fibre can be removed using mechanical stripping. However, the fibre coating must be removed carefully to avoid any damage. A stripping tool can cause scratches and surface flaws, which are the main reasons of fibre transmission losses/failures. In the case of ZBLAN fibre, however, chemical stripping is required, which is comparatively reliable compared to mechanical stripping and the fibre has relatively less chances to sustain surface defects. In this experiment we used dichloromethane to remove the coating of ZBLAN fibre to the desired length. After stripping, both types of fibre were cleaned with Acetone to remove any surface particles.

4.1.3 Connector end face preparation

End surface quality is one of the most important factors affecting fibre losses. Quality end faces can be obtained by polishing or by using a fibre cleaver. Polishing is employed in connector terminations when the fibre is secured in a ferrule by epoxy. We have different types of connectors, but we used PC connectors in our experiment due to compatibility with source and receiver.

Once the optical fibre is terminated with a connector, the connector end face preparation will determine the connector return loss (also known as back reflection). The back reflection is the ratio between the light propagating from the source in the forward direction and the light reflected back into the light source.

4.2 Facet Polishing of Si/ZBLAN Fibre

There are mainly three types of polishing, and these are briefly explained below [45].

1- **Physical Contact Polish:** One of the most popular methods for connectorization is physical contact polishing. In PC polish the polished surface is slightly curved rather flat resulting in better contact by eliminating the air between interfaces. This type of polishing results in a loss of almost -30 to -40 dB

2- **Super/Ultra Physical Contact Polish:** High speed optical transmission uses this polishing method where surface quality of the connector is improved to reduce back reflections. This type of polishing results in a loss of -40 dB to less than -55dB

3- **APC Polish:** Angle Polished Connectors are the most efficient connectors as they pose least loss of signal (less than -60dB). In APC, the facet is polished at 8 degrees to provide an angle to end surface of connector [45].

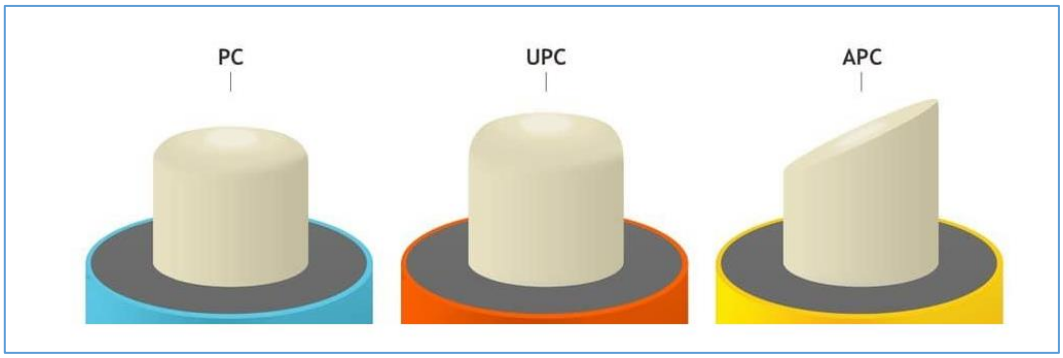

Figure 4.1: Connectors end faces (PC, UPC, APC)

Flat Polishing is another method where the fibre surface is flat polished rather than curved or angled, but this results in a higher loss (back reflection of about -16 dB).

After fibre stripping and securing the fibre in ferrule by using epoxy Norland 61, UV light was shined to fix the fibre properly in ferrule. Once the epoxy cured, excess fibre was removed from the ferrule. After fixing the fibre in the connector, the next step was the facet polishing of the fibre. First, the fibre was fixed in a polishing holder which was made of stainless steel. We used SFP-700 fibre polisher Seikon Giken in our experiment for the facet polishing of the sample. The polishing material consists of the three elements detailed below.

Polishing film: There are four different types of polishing films used for this experiment, which are listed in Table 4.1.

Polishing film	Application of films	Usage of films	Duration of Polishing(seconds)
30 µm Diamond film	Coarse polishing	1 time	30
6 µm Diamond film	Rough polishing	10-20 times	60
1 µm Diamond film	Medium polishing	10-20 times	60
1 µm Al_2O_3 film	Final polishing	1 time	30

Table 4.1: Types of Polishing films, their applications and usage

Polishing Pads: Polishing pads of different thickness, material and hardness are available. For flat polishing, glass polishing pads are usually used but for convex polishing, neoprene polishing pad are a mandatory requirement.

Installation: For installing the surface of the polishing pad, the polishing film and the turntable were cleaned with lint-free tissues and alcohol to ensure the removal of any particles from the surfaces. After cleaning, the polishing film on the polishing pad was placed with the abrasive side facing up and a fibre holder was placed on top, which can secure six fibre connectors at a time. A fibre connecter was connected to one of the slots and a timer was used to enable polishing times to be controlled precisely. All polishing films listed in table above were used sequentially in descending order of roughness to achieve the desired surface with minimal losses.

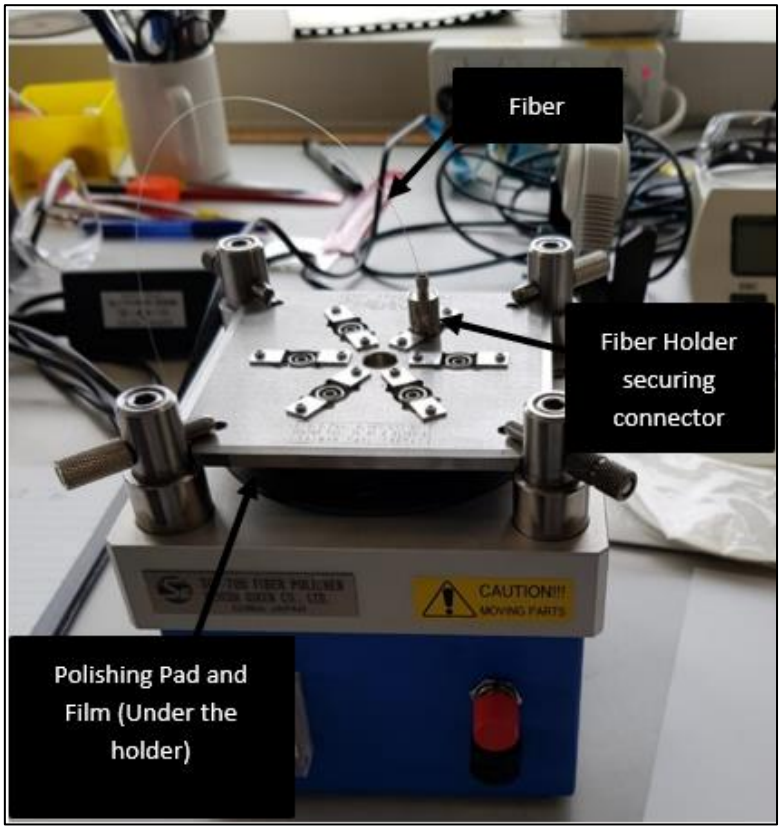

Figure 4.2 Setup SFP-700 fibre polisher Seikon Giken for facet polishing of fibre.

The following picture shows a microscopic image of the facet polishing of Si fibre with core of 9 µm and a cladding diameter of 125 µm at 40x magnification.

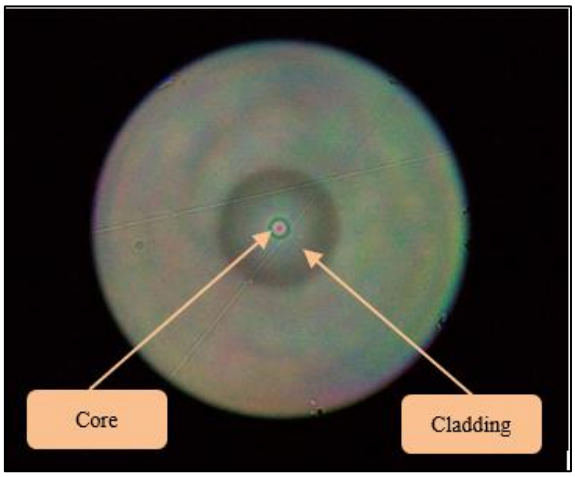

Figure 4.3 Microscopic view of facet of a polished fibre.

4.3 Side Polished Fibre

A portion of the jacket is removed from the middle of the fibre sample so that the fibre can act as a three-layer waveguide [45]. The first layer in a three-layer waveguide is the core, with a high

refractive index. The second layer is polished cladding, with a refractive index lower than the core. Due to the reduced thickness, the cladding evanescent field of the fibre is accessible through the polished surface of fibre. Any material in contact with this surface acts as a third layer. In case of no material pasted on the polished surface, air acts as the third layer, with a refractive index of 1. If the refractive index of the pasted material is equal to or higher than the cladding, the fibre suffers from high loss due to leakage of light through this region. This leakage of light is due to evanescent field absorption in the polished region, which is an exponentially decaying field from the surface of the core towards the outer cladding, as shown in Figure 4.4 below. If the refractive index of the material in contact with the polished surface is lower than the cladding, then power transmitted through the fibre increases due to low losses from the polished region [6][46].

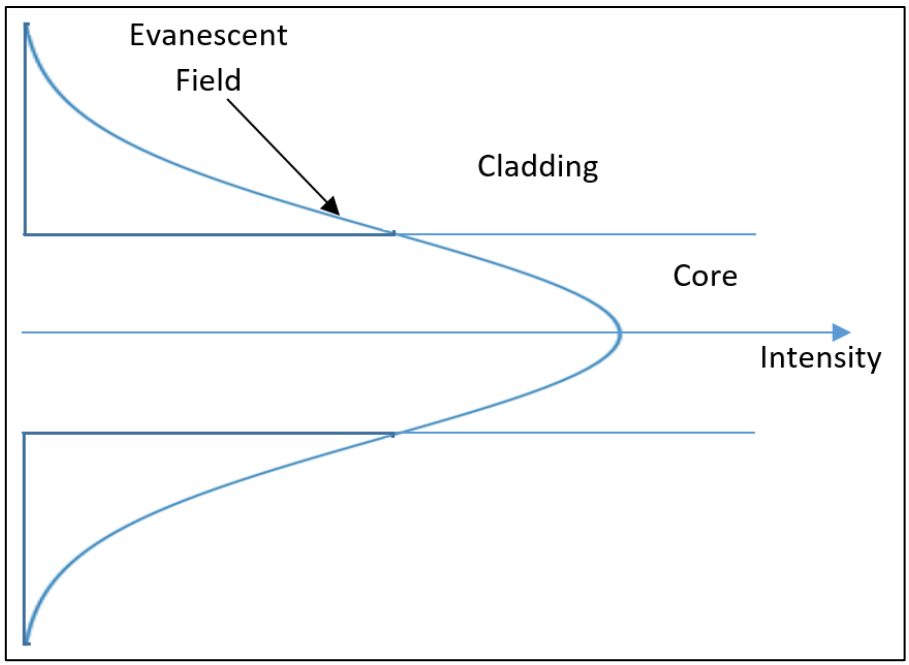

Figure 4.4: Evanescent field in an optical fibre.

The handling of the fibre is one of the most important factors during the side-polishing procedure. Extreme precision is required while designing and during experimental procedures due to the fragility of the fibre. Another challenge is to control the depth of grinding towards the core to access the evanescent field at a desirable distance from the core. Many methods have been tried to side polish a fibre with accuracy and consistency, but a reliable method has not yet been discovered that can generate consistent results. However, in our experiment we will discuss techniques used to accurately side polish fibres.

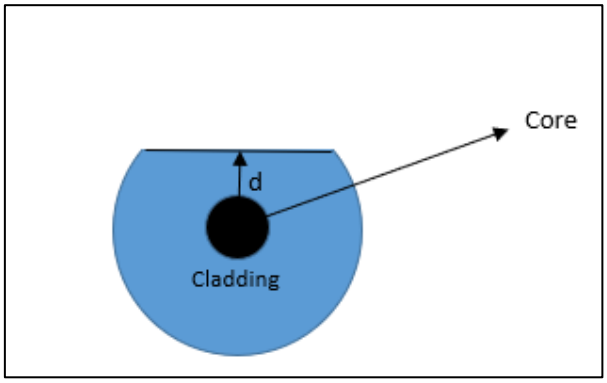

Figure 4.5 Side polished fibre and distance from core to access evanescent field.

4.3.1 Logitech PM5 lapping and polishing machine for SPF

For the purpose of the side polishing of a fibre we used a Logitech PM5 lapping/polishing machine. To support fibre during polishing/lapping, custom designs are needed. The Logitech PM5 machine is used to polish various material with extreme precision (up to 1-micron accuracy). According to the material to be polished, various abrasives and polishing plates can be used for the purpose of grinding. The sample to be polished is mounted on a polishing jig using a metal mounting plate, and the jig is inverted and placed on the grinding wheel of the Logitech PM5. Both pressure and revolution speed can be controlled for desired polishing. The following section elaborates the side polished fibre and customized designs used to provide stability to the fibre during the polishing process [47].

4.3.2 Custom design

Optical fibres are too small and fragile to be polished alone, so a means to support the fibre during polishing is required. To keep the fibre in place, many investigators used different precision engraving tools to support the fibre during side-polishing. We have used customized 3D-models and v-grooved silica slides to serve the purpose [48]-[50].

4.3.2.1 3D-model

In order to have consistency in results and improve the handling of fibre during the experiment, a custom designed 3D model was used to harness the fibre for the purpose of polishing. The material used to build the 3D model was ABS (acrylonitrile butadiene styrene) [51], which is one of the most popular among 3D printing filaments to build durable structures because of its properties to withstand high pressure and high temperatures.

A 3D model was built in Google SketchUp, which is used as a modelling tool in many industries, including landscape architecture, interior design, and civil and mechanical engineering. The primary

reason to build a 3D model was to create a block in which fibre does not have to pass through any sharp bends, as with the high-pressure during grinding or polishing, fibre can get damaged from sharp edges. Figure 1 below shows the 3D model built to secure the fibre for polishing.

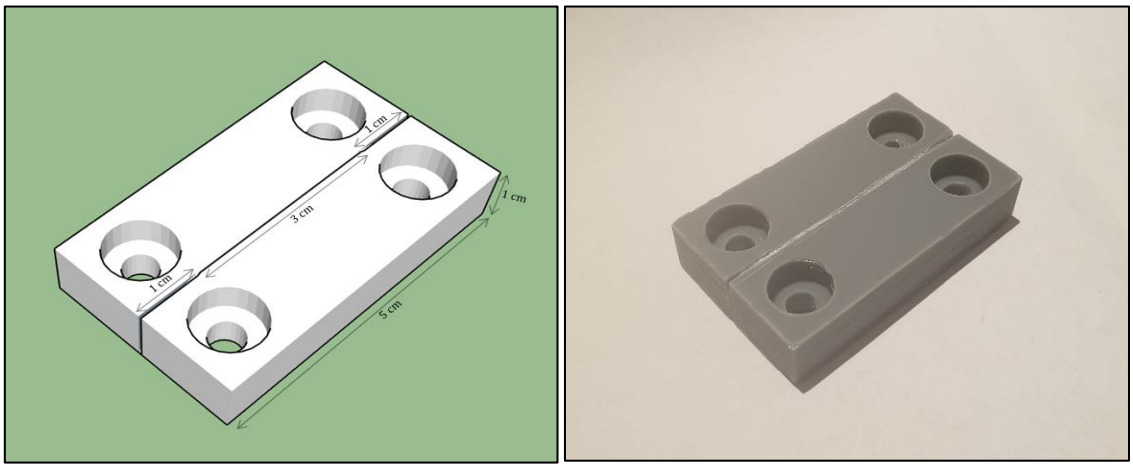

Figure 4.6 3D model in Google SketchUp and a printed 3D sample.

As can be seen from the figure above, a 3 cm groove of a smaller size (a rectangular shape with 130 µm of width and 100 µm depth) is left in the middle to rest the non-jacketed fibre on (125 µm diameter enclosing 9 µm core). The depth of the groove was set to 100 µm in order to remove 25 microns (40% of a side) above the surface of the 3D model during the grinding process. Multiple 3D models were printed for various depths of the groove; hence, achieving various depths of grinding. The grinding process continued until losses started to increase during the grinding process and a continual monitoring through 1550nm portable power meter was required to indicate that we had accessed the evanescent field. A 1 cm groove with a width 450 µm on both sides of the sample were left to guide the fibre down from the sample without any sharp bends. This groove was curved from the base, as shown in Figure 4.6. There were four holes left in the corners for screws (1 cm head and 0.5 cm screw) to fix the sample on a mounting plate.

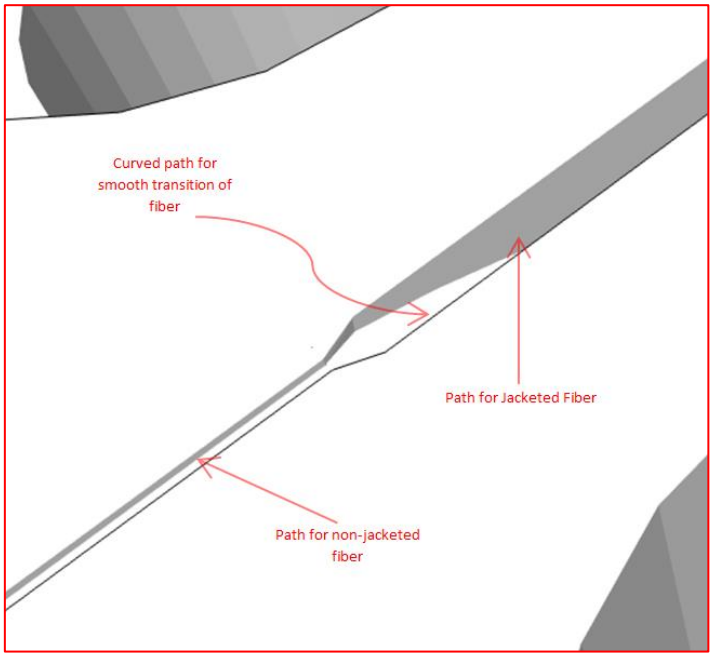

Figure 4.7 Path of jacketed and non-jacketed fibre and smooth transition to avoid sharp bend.

Before grinding, the samples were screwed to a mounting plate. To polish the fibre a 3 cm portion from the middle of the sample was prepared as in the above section and was stripped and cleaned with acetone. The unjacketed fibres were placed in 3D-model grooves and were held by epoxy. In our experiment, Norland-63 was used to achieve adhesion, toughness, and durability. Epoxy was first applied to the central section of a fibre. The fibre sections in the outer regions were glued after the epoxy in the central region was dry and hard. Such a precaution was necessary to minimize the possible movement of the fibre near the central region during the experiment. Repeated observations with optical microscopes were made to ensure that fibre in the central region sat properly in the groove.

4.3.2.2 V-grooved glass slide

The second sample used in our experiment to hold the fibre was a v-grooved laser-machined silica slide to keep the fibre from any displacement during the experiment. The fibre was secured in the v-groove of the silica slide using Epoxy Norland-61. In the next step, the sample was placed in a UV chamber to secure the fibre more firmly in groove. A small amount of wax was applied on both the glass slide and the mounting plate to glue both the slide and mounting plate.

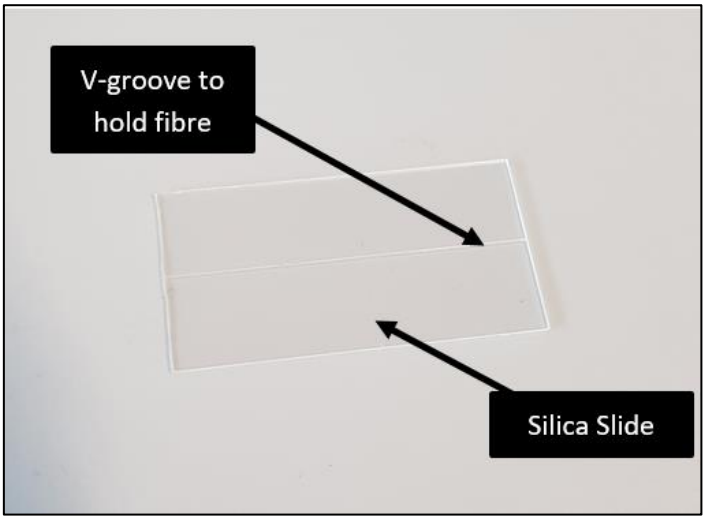

Figure 4.8: V-grooved glass slide to secure the fibre for side-polishing.

4.3.2.3 Mounting plate

The next step was to design the mounting plate to hold the sample within the polishing jig, and it was also designed using Google Sketch Up. A mounting plate was designed so that it could be connected to the polishing jig of the Logitech machine, and the top of the mounting plate could hold our 3D model through the screws, and the silica slide could also be attached using wax. Side grooves were also left on the mounting plate for a continuous fibre path out from the jig without any sharp bends. The following figure illustrate the 3D model of the mounting plate.

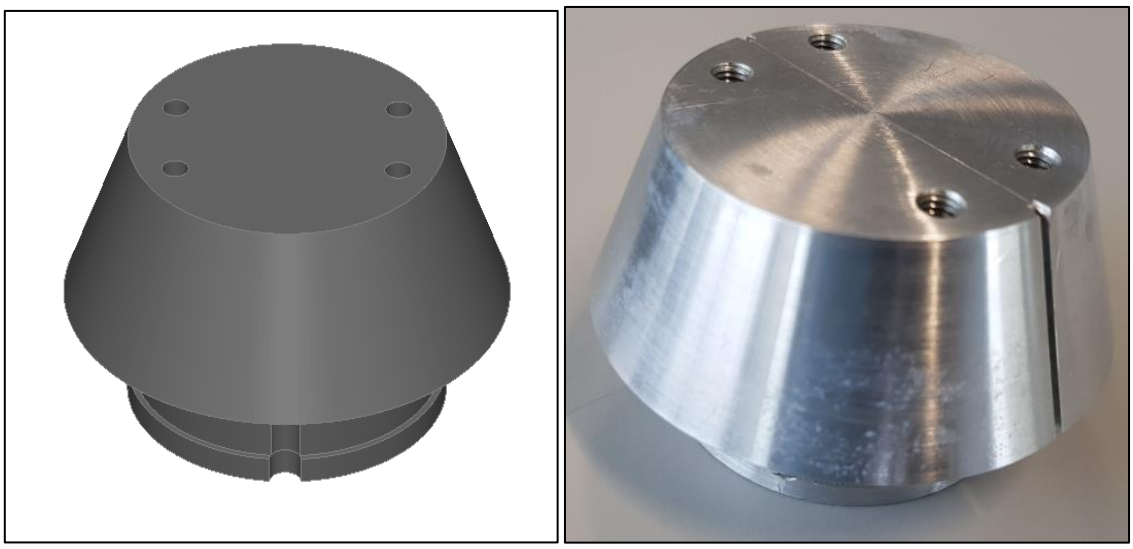

Figure 4.9 3D Model of mounting plate in google Sketchup and manufactured sample.

4.3.3 Lapping/grinding and polishing

Once the fibres were glued properly on to the custom designs, the sample was fixed on the mounting plate. The mounting plate was secured into the PP5 polishing jig (Logitech, Scotland), and the fibre coming out from the sample was threaded through slots in the jig sides and were wound safely at the top of the jig. The back reflection of a He-Ne laser beam, from the glass puck via a 3.2 m beam path was used to align the sample surface with the grinding plate to ensure even grinding across all sides of the sample.

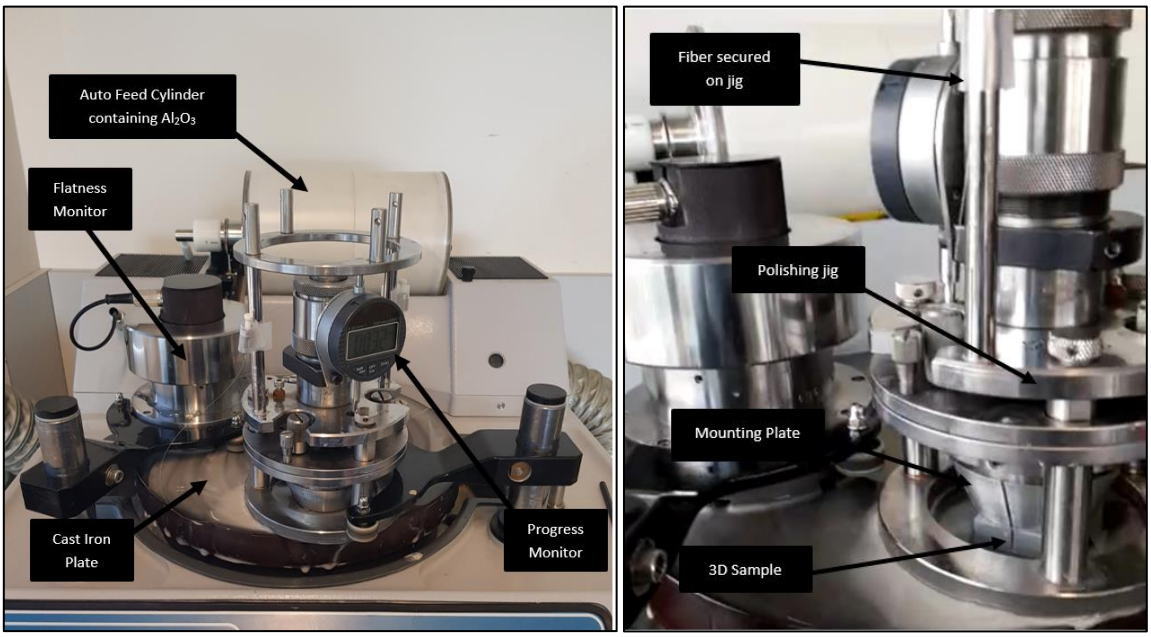

Figure 4.10: Logitech PM5 used for side polishing using custom 3D model.

The polishing jig applies pressure in the vertical direction during grinding and polishing, which can be adjusted to change the time to achieve the desired depth of grinding. The lower the pressure, the more time is required to achieve the desired depth of grinding, and the depth of grinding can be controlled more easily. The pressure also has an impact on the sample, for example, using high pressure would exert more force on our sample, and because of this the fibre can get chipped, especially from the edges where the fibre comes out of the sample. Fixing the fibre in the groove properly and the alignment of the sample with the grinding plate is very important as the sample also experiences strong forces in almost every direction on the horizontal axis, as the jig revolves around its axis as well as around the axis of the grinding plate. If the fibre is not properly glued within the sample, this angular force can cause the fibre to dislocate from its position and break. Figure 4.11 shows all the forces experienced by the sample during the experiment.

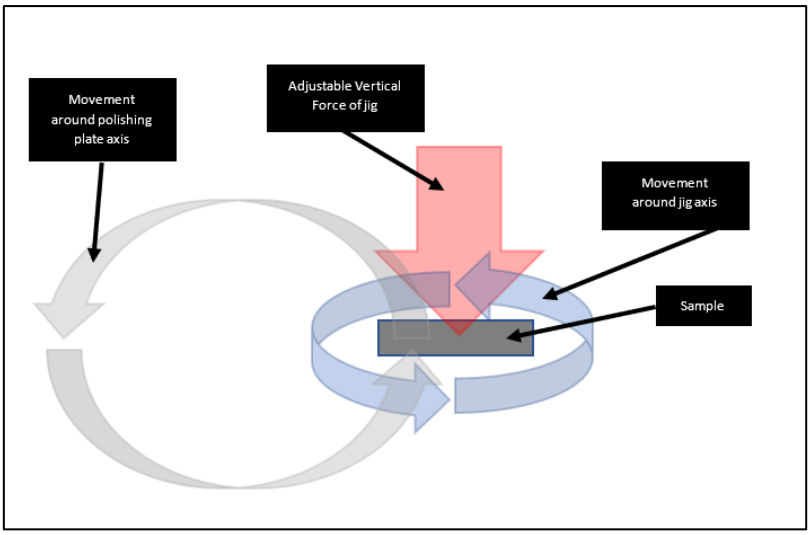

Figure 4.11: Forces and movement of sample while grinding on Logitech PM5.

For the purpose of grinding, Al_2O_3 powder was selected, which was mixed with filtered tap water and fed to the grinding plate through an auto-feed cylinder on top of the Logitech machine. The 5 micron abrasive powder was used to grind the surface of cladding. Machine settings were kept at lower revolutions and a lower pressure to avoid any damage. Input from the source (Mooseine 1550 nm Single Mode Laser Light) was set to -6.5 dBm at 1550 µm, and output was continuously monitored by stopping the machine at different layer removals through metered measurement (Power Meter - 0.01 dB Resolution, Calibrated At 1550 nm).

Multiple samples were generated with various depths of grinding (25 microns to 40 micron), resulting in certain losses against each grinding. To finalize the finishing of the surface of the fibre, 3-micron polycrystalline diamond lapping solution (UltraSol) was used to achieve a smooth surface. Before using UltraSol, the fibre surface needed to be cleaned to avoid any contamination Surface smoothness was also important for the next step, as we pasted saturable absorber on the side polished fibre. There should be no air between the pasted material and surface of fibre to avoid any losses.

Results and discussion

The experiment was attempted multiple times to achieve the desired depth and surface of the side polished fibre using custom samples as mentioned in the previous section. The results are shown in Figure 4.12.

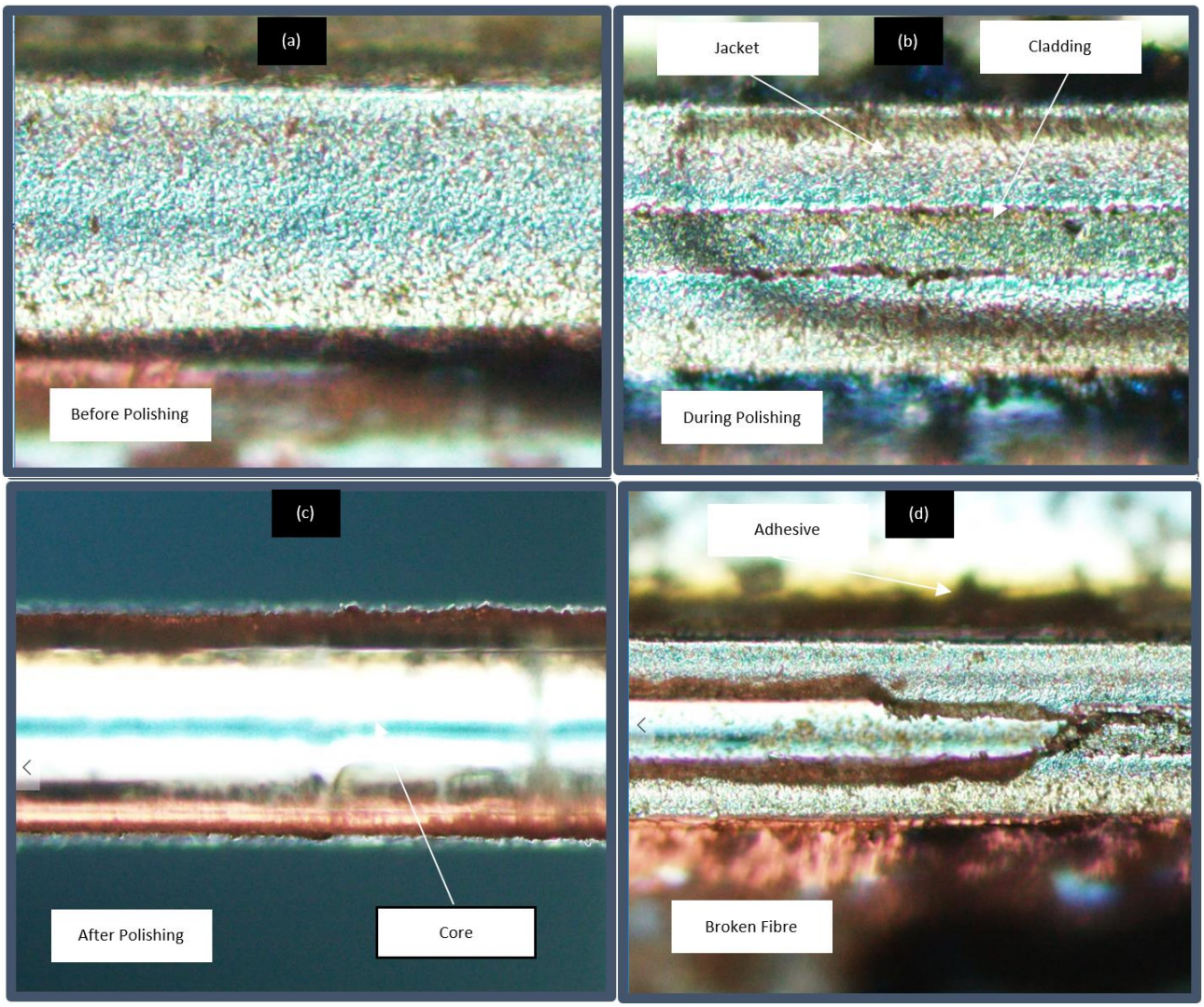

Figure 4.12: SPF results using Logitech machine: (a) before polishing (b) surface during polishing (c) surface after polishing (d) broken fibre during one of the attempts.

Attempts to side polish the fibre were made with and without an external jacket. The above images show the results of the fibre being used with a jacket, where the first jacket is polished and then the cladding is gradually removed to achieve the desired results. The reason for using fibre with a jacket was to strengthen the fibre while polishing through the Logitech machine, thus reducing the chances of damaged fibre. Figure 4.12 (b) shows the polished surface of the fibre during the process of polishing, and Figure 4.12 (c) shows the image of a polished surface which is comparatively smooth to the surface of that shown in Figure 4.12 (b). Many attempts were made to achieve the desired

results during which our fibre was broken due to several reason. Figure 4.12 (d) shows one of the failed attempts, in which the fibre was broken during the polishing process. Table below shows the attempts of polishing

Work is still in progress to achieve the most favourable distance from the core, along with the smooth surface for printing material on the SPF.

Polishing attempt number	Input Reading from Source (dbm at 1550nm)	Output reading from Power Meter before polishing (dbm at 1550nm)	Output reading from Power Meter after polishing (dbm at 1550nm)	Polishing Depth (microns)
1	-6.5	-6.8	-15.2	35
2	-6.5	-7.1	-28.5	45
3	-6.5	-6.5	-58.0 (Broken)	55
4	-6.5	-7.4	-58.5 (Broken)	50

Table 4.2 Results of side polishing at various depths

4.4 Chapter Summary

The chapter explained the experimental setup and procedures used to polish silica/fluoride fibre. A customized design was applied as an innovative approach to achieve consistent and reliable results using a Logitech PM5 lapping and polishing machine. A 3D sample was printed to harness a 3 cm portion of the fibre which was to be polished. A custom mounting plate compatible with the Logitech PM5 polishing jig was also designed to fix the 3D sample onto the mounting plate. Al_2O_3 abrasive powder (5 micron) solution was used on the iron cast plate of the machine to grind the sample and then UltraSol was used to finish the final polishing so as to achieve a smooth surface. The same experiment was also carried out with a v-grooved silica slide pasted on the mounting plate, rather than using a 3D model.

5

Conclusion and Future Work

In the past decade, silica fibre doped with rare earth elements have produced promising results, acting as a lasing medium with low phonon energy; thus, resulting in low losses, specifically at the low-infrared range. This is the reason silica fibre has been used in diverse applications ranging from fibre lasers to telecommunication networks [52]. For molecular spectroscopy, imaging, and detection purposes we have to move to mid-infrared wavelengths as they show better absorption properties for many common materials [53]-[54]. The size of mid-infrared equipment is the biggest constraint and is preventing it being available for routine industrial usage. The present project is an important step towards development of a compact mid-infrared fibre laser (all fibre laser) using nanomaterial, such as MXene and PtSe2.

Chapter 3 demonstrated the stable mode-locked pulses achieved through fibre laser based on a Fabry-Perot laser cavity and 2D nanomaterial being used in the confocal setup external to the fibre. It also explained the broadening of the spectrum due to the use of saturable absorber material (pasted on the CaF2 substrate) within the confocal setup. Results were recorded for different layers of saturable absorber and proved to be promising as regards achieving stable mode-locked pulses. It was also observed that the signal to noise ratio improved through the increased number of layers of saturable absorber used.

The next step was an improvement to the existing experimental setup so as to further reduce the size of the laser through side polishing and printing nanomaterial on the polished surface rather than having it in a confocal setup. For this purpose, a Logitech PM5 was used with custom models to hold the fibre in the polishing jig for side polishing. 3D printed models and grooved glass slides were used as fibre holders within the polishing jig, and constant monitoring was conducted throughout the experiment to check if the evanescent field was accessible. Work is still in progress to achieve the smooth polished surface of the fibre, along with the optimum distance required between the polished surface and the fibre core so that material can be printed on the surface to act as a saturable absorber for a compact mid-infrared fibre laser.

5.1 Future Works

With the successful generation of stable mode-locking, as demonstrated in Chapter, 3 using novel 2D nanomaterial, we can expect that the same results can be achieved by side polishing a fibre and pasting nanomaterial on the surface to interact with the evanescent field. For this purpose, we have developed techniques for reliable side-polishing of fibre using a Logitech PM5. The future works are associated with the printing of nonmaterial on the polished surface of the fibre and recording the results for various layers of printing so as to achieve the same results as we attained in Chapter 3. The inkjet printing method will be used to print the material on the polished surface of the fibre. Figure 5.1 shows an expected setup after printing material on the polished surface of the fibre. If we compare it with Figure 3.1 in Chapter 3, we can notice the avoidance of most of the optical components.

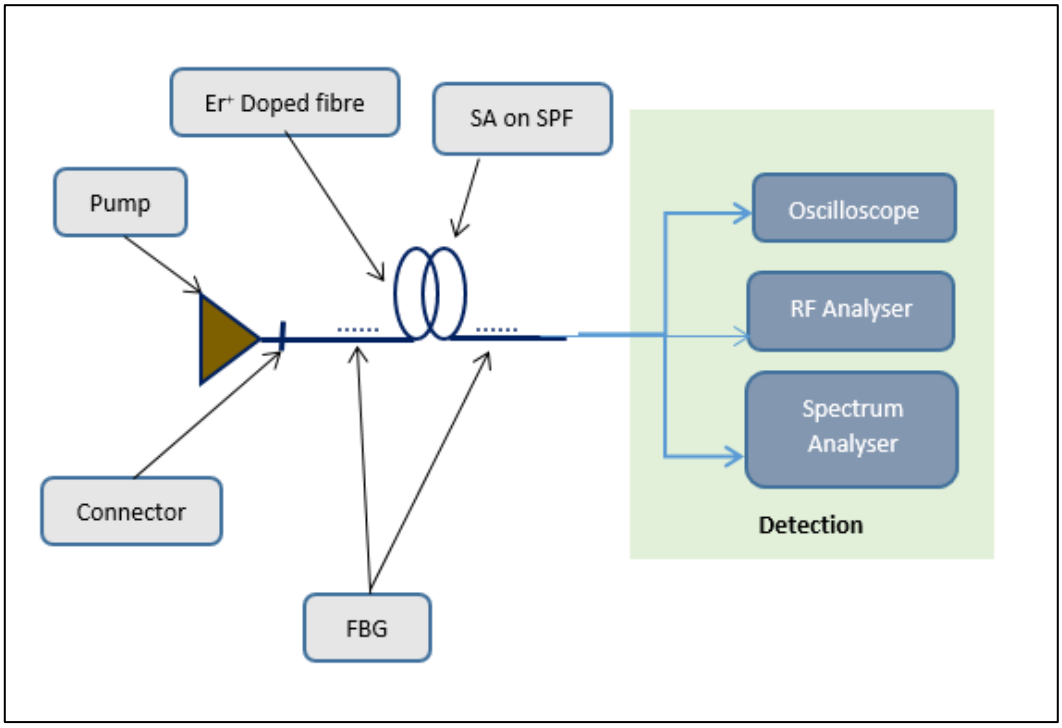

Figure 5.1 Future setup to achieve mode-locking through SPF.

Such ultra-compact photonic devices which are built based on the evanescent field are called evanescent field devices. In future, because of these devices, we would be able to produce ultra-compact photonic equipment for diverse industrial applications.

References

[1] G. Bharathan, R.I. Woodward, M. Ams, D.D. Hudson, S.D. Jackson, “Direct inscription of Bragg gratings into coated fluoride fibres for widely tunable and robust mid-infrared lasers“, Optics express 25 (24), 30013-30019 (2017)

[2] M. J. F. Digonnet and H. J. Shaw, "Analysis of a tunable single mode optical fibre coupler”, IEEE J. Quantum Electron, QE-18, 746-754 (1982)

[3] S. Markatos, S. Ayres, D. Kreit, A. Kerr, R. C. Youngquist, and I. P. Giles," Optical fibre switch”, in Fibre Optic Sensors II,A. M. Scheggi, ed., Proc. Soc. Photo-Opt. Instrum. Eng 798, 376-380 (1987).

[4] B. F. Lamouroux, A. G. Orszag, B. S. Prade, and J. Y. Vinet," Continuous laser amplification in a monomode fibre longitudinally pumped by evanescent field coupling”, Opt. Lett. 8, 504-505 (1983).

[5] S. A. Newton, K. P. Jackson, and H. J. Shaw," Optical fibre V-groove transversal filter”, Appl. Phys. Lett. 43, 149-151 (1983).

[6] S.M. Tseng and C.L. Chen, “Side-polished fibres”, Appl. Optics, 31, pp. 3438-3447 (1992)

[7] G.R. Gordon, "The LASER, Light Amplification by Stimulated Emission of Radiation”, In Franken, P.A. and Sands, R.H. (Eds.).The Ann Arbor Conference on Optical Pumping, the University of Michigan, pp.1281959.

[8] Siegman, E.Anthony, “Lasers”, Revised ed. edition, (1986). Pp. 2. ISBN 978-0-935702-11-8

[9] F. Mitschke, “Fibre Optics.Physics and Technology”, Springer-Verlag Berlin Heidelberg, (2016)

[10] T.Hu, Ultrafast Mid-infrared Fibre Lasers, PhD, University of Sydney, 2015

[11] A. W. Snyder and J. D. Love, “Optical waveguide theory”, Springer, 1996.

[13] I.A. Bufetov and E.M. Dianov, “Bi-doped fibre lasers” Laser Phys. Lett. 6 487–504 (2009)

[14] E. Snitzer, “Optical Maser Action of Nd + 3 in a Barium Crown Glass” Phys. Rev. Lett. 7 444–6, (1961)

[15] S. Kawakami, S. Nishida, "Characteristics of a doubly clad optical fibre with a low-index inner cladding". IEEE Journal of Quantum Electronics. 10 (12): 879–887, (1974).

[16] R. Allen and L. Esterowitz, “CW Diode Pumped 2.3 μm Fibre Laser”, Applied Physics Letters 55(8), 721 (1989).

[17] M. C. Brierley and P. France, “Continuous wave lasing at 2.7 Âtm in an erbium-doped fluoro zirconate fibre”, Electronics Letters 24(8), 935 (1988).

[18] O. Henderson-sapir, J. Munch, and D. J. Ottaway, “A Higher Power 3.5 μm Fibre Laser”, Advanced Solid State Lasers (ASSL) OSA, 5 (2014).

[19] L.Wetenkamp, “Efficient CW operation of a 2.9 Âtm Ho3+- doped fluoro zirconate fibre laser pumped at 640 nm”, Electronics Letters 26(8), 883 (1990).

[20] C. Carbonnier, H. Tobben, and U. B. Unrau, “Room temperature CW fibre laser at 3.22 μm”, Electronics Letters 34(9), 893 (1998).

[21] J. Schneider, C. Carbonnier, “Characterization of a Ho 3+ -doped fluoride fibre laser with a 3.9 Âtm emission wavelength”, Applied Optics 36(33), 8595 (1997).

[22] M. R. Majewski and S. D. Jackson, “Highly efficient mid-infrared dysprosium fibre laser”, Optics Letters 41(10), 2173 (2016).

[23] J. Li and S. D. Jackson, “Numerical Modeling and Optimization of Diode Pumped Heavily-Erbium-Doped Fluoride Fibre Lasers”, IEEE J. Quantum Electron. vol. 48, pp. 454-464, Apr. 2012.

[24] C. K. N. Patel, “Continuous-wave laser action on vibrational–rotational transitions of CO2”, Phys. Rev. 136 (5A), A1187 (1964).

[25] Silfvast, T. William, “Laser Fundamentals, Cambridge University Press”, (1996).

[26] M.G. Littman, X. Wang, “Pulsed Lasers”, Experimental Methods in the Physical Sciences, 29, 1079-4042, (1997)

[27] R.W. Hellwarth, “Control of fluorescent pulsations, in Advances in Quantum Electronics”, ed.by J.R. Singer , pp. 334–341, (1961)

[28] J. Hecht, “Understanding Fibre Optics”, 5th edition, Laser Light Press, (2015)

[29]W. E. Lamb, “Theory of an optical laser”, Phys. Rev. 134 (6A), A1429 (1964)

[30] L.E. Hargrove, R.L. Fork, and M.A. Pollack, “Locking of He-Ne laser modes induced by synchronous intracavity modulation”, Appl. Phys. Lett., 5, 4–5, (1964).

[31] D. Kuizenga and A. Siegman, “FM and AM mode locking of the homogeneous laser”, IEEE J. Quantum Electron., 6, 694–708, (1970).

[32] H. Haus, “A theory of forced mode locking”, IEEE J. Quantum Electron., 11, 323–330, (1975).

[33] A. Sobiesierski, P.M. Smowton, “Devices and Applications in Comprehensive Semiconductor Science and Technology”, (2011).

[34] R. R. Gattass, E. Mazur, Nat. “Photonics”, 2, 219, (2008)

[35] S. A. Diddams, L. Hollberg, V. Mbele, “Nature”, 445,627, (2007).

[36] R. D. Vivie-Riedle, U. Troppmann, “Femtosecond Lasers for Quantum Information Technology”, Chem. Rev. 2007, 107, 5082.

[37] B. G. Kim et al., “Nonlinear Bragg reflector based on saturable absorption”, Appl. Phys. Lett. 54, 1095 (1989)

[38]Young In Jhon, Joonhoi Koo, Babak Anasori, Minah Seo, Ju Han Lee, Yury Gogotsi, and Young Min Jhon, “Metallic MXene Saturable Absorber for Femtosecond Mode-Locked Lasers”, (2017).

[39]L.Tao, X.Huang, J.He, Y Lou, L.Zeng, Y.Li, H.Long, J.Li, L.Zhang and Y.Hong, “vertically standing PtSe2 film: a saturable absorber for a passively mode-locked, Nd: LuVO4 laser”, (2018).

[40] Bharathan, G., Woodward, R. I., Ams, M., Hudson, D. D., Jackson, S. D., and Fuerbach, A., “Direct inscription of Bragg gratings into coated fluoride fibres for widely tunable and robust mid-infrared lasers”, Opt. Express 25(24), 30013 (2017).

[41] Bharathan, G., Fernandez, T. T., Ams, M., Woodward, R. I., Hudson, D. D., and Fuerbach, A., “Optimized laser-written ZBLAN fibre Bragg gratings with high reectivity and low loss”, Opt. Lett. 44(2), 423 (2019).

[42] Jie Ma, Zhipeng Qin, Guoqiang Xie , Liejia Qian, and Dingyuan Tang , “Review of mid -infrared mode-locked laser sources in the 2.0 μm–3.5 μm spectral region” (2019)

[43] https://www.rp-photonics.com/transform_limit.html

[44] Jeff Hecht, “Understanding Fibre Optics”, 5 edition (April 29, 2005)

[45] J. Hu and C. R. Menyuk, “Understanding leaky modes: slab waveguide revisited”, Advances in Optics and Photonics, vol. 1, no. 1, p. 58, Jan. 2009.

[46] Tang J, et al., “Fabrication of side-polished single mode-multimode-single mode fibre and its characteristics of refractive index sensing”, IEEE J Sel Top Quantum Electron 23(2), 238(2017).

[47] S.Gross, “Direct-Write Mid-IR Waveguide Lasers” (2012).

[48] S.Tseng, C.Chen, “Side polished fibre”, applied optics, vol.31, No.18 (1992)

[49] S. A. Newton, K. P. Jackson, and H. J. Shaw, “Optical fibre V-groove transversal filter”, Appl. Phys. Lett. 43, 149-151 (1983).

[50] M. J. F. Digonnet, J. R. Feth, L. F. Stokes, and H. J. Shaw, "Measurement of the core proximity in polished fibre substrates and couplers”, Opt. Lett. 10, 463-465 (1985).

[51] “Plastic Properties of Acrylonitrile Butadiene Styrene (ABS) at the Wayback Machine Small table of ABS properties towards the bottom” Archived May 15, 2010,. Retrieved 7 May 2010

[52] Vivek Singh, Pao Tai Lin, Neil Patel, Hongtao Lin, Lan Li, Yi Zou, Fei Deng , “Mid-infrared materials and devices on a Si platform for optical sensing” , Sci Technol Adv Mater (2014)

[53] Yu Z., and Fan S, “Extraordinarily high spectral sensitivity in refractive index sensors using multiple optical modes”, Opt. Express; 19:10029 (2011).

[54] Farca G, Shopova S I., and Rosenberger A T, “Cavity-enhanced laser absorption spectroscopy using microresonator whispering-gallery modes”, Opt Express. 15, 17443 (2007).

[55] P.Liao , C.Bao , A.Almaiman , A.Kordts , M.Karpov , M.Hubert , “Demonstration of Multiple Kerr-Frequency-Comb Generation Using Different Lines From Another Kerr Comb Located Up To 50 km Away”, IEEE PTL 31 ,1409 (2019).

[56] C. Frerichs and T. Tauermann, “Q-switched operation of laser diode pumped erbium-doped fluorozirconate fibre laser operating at 2.7 μm,” Electron. Lett. 30(9), 706–707 (1994).

[57] S. Tokita, M. Murakami, S. Shimizu, M. Hashida, and S. Sakabe, “12 W Q-switched Er:ZBLAN fibre laser at 2.8 μm,” Opt. Lett. 36, 2812–2814 (2011).

[58] T. Hu, D. D. Hudson, and S. D. Jackson, “Actively Q-switched 2.9 μm Ho3+ Pr3+ -doped fluoride fibre laser,” Opt. Lett. 37, 2145 (2012).

[59] J. T. Hu, and S. D. Jackson, “Q-switched induced gain switching of a two-transition cascade laser,” Opt. Express 20(12), 13123-13128 (2012).

[60] M. Gorjan, R. Petkovsek, M. Marincek, and M. Copic, “High-power pulsed diode-pumped Er:ZBLAN fibre laser,” Opt. Lett. 36(10), 1923-1925 (2011).

[61] C. Frerichs and U. B. Unrau, “Passive Q-switching and mode-locking of erbium-doped fluoride fibre lasers at 2.7 μm,” Opt. Fibre Technol. 2, 358–366 (1996).

[62] C. Wei, X. Zhu, R. A. Norwood, and N. Peyghambarian, “Passively Q-Switched 2.8-μm Nanosecond Fibre Laser, ” IEEE Photon. Technol. Lett. 24, 1741-1744 (2012).

[63] U. Keller, K. J. Weingarten, F. X. Kartner, D. Kopf, B. Braun, I. D. Jung, R. Fluck, C. Honninger, N. Matuschek, and J. A. d. Au, “Semiconductor saturable absorber mirrors (SESAMs) for femtosecond to nanosecond pulse generation in solid-state lasers”, IEEE J. Sel. Top. Quantum Electron. 2(3), 435-453 (1996).

[64] A. Haboucha, V. Fortin, M. Bernier, J. Genest, Y. Messaddeq, and R. Vallée, “Fibre Bragg grating stabilization of a passively mode-locked 2.8 μm Er3+: fluoride glass fibre laser,” Opt. Lett. 39(11), 3294-3297 (2014).

[65] J. Li, D. D. Hudson,Y. Liu, and S. D. Jackson, “Efficient 2.87 μm fibre laser passively switched using a semiconductor saturable absorber mirror,” Opt. Lett. 37(18), 3747-3749 (2012).

[66] Bo Guo, “2D noncarbon materials-based nonlinear optical devices for ultrafast photonics”, Chinese Optics letters. 16(2), 020004 (2018).

[67] S.Ning, G.Feng, S.Dai, H.Zhang, W.Zhang, L.Deng, and S.Zhou , “Mid-infrared Fe^{2+} :ZnSe semiconductor saturable absorber mirror for passively Q-switched Er3+-doped ZBLAN fibre laser”, AIP Advances. 8, 025121 (2018).

[68] W.Li, H.Wang, T.Du, B.Xu, Z.Cai, H.Xu and Z.Luo, “Compact self-Q-switched, tunable mid-infrared all-fibre pulsed laser”, Optics Express. 26(26), 34497 (2018).

[69] Q. Wu, X. Jin, S. Chen, X. Jiang, Y. Hu, Q. Jiang, L. Wu, J. Li, Z. Zheng, M. Zhang and H. Zhang, “MXene-based saturable absorber for femtosecond mode-locked fibre lasers” ,Optics Express. 27(7), 10159 (2019).

[70] T.Hu, D.D. Hudson, and S.D.Jackson, “Stable, self-starting, passively mode-locked fibre ring laser of the 3 μm class”,OSA. 39, 2133-2136 (2014).

[71] S.Duval, M.Bernier, V.Fortin, J.Genest, M.Piche and R.Vallee, “femtosecond fibre lasers reach the mid-infrared”, Optica. 2(7), 623 (2015).

[72] R. I. Woodward,a M. R. Majewski, and S. D. Jackson, “Mode-locked dysprosium fibre laser: Picosecond pulse generation from 2.97 to 3.30 μm”, APL Photonics. 3, 116106 (2018).

[73] X.Lai, J.Li , H.Luo1, C.Zhu, Y.Hai1, Y.Shi1, Y.Gao1 and Y.Liu, “ High power passively Q-switched Er3+- doped ZBLAN fiber laser at 2.8 μm based on a semiconductor saturable absorber mirror” 8 Laser Phys. Lett. 15, 085109 (2018).